PALACKÝ UNIVERSITY OLOMOUC

DEPARTMENT OF PHYSICAL CHEMISTRY

Faculty
of Science

Experimental studies of interactions of cells with newly developed graphene derivatives

MASTER'S THESIS

Bc. JAN BELZA

Supervisor: Mgr. Kateřina Poláková, Ph.D.

Study programme: N1407 Chemistry
Subject of study: Physical chemistry
Form of study: Full-time

Olomouc 2018

DECLARATION

I declare that I elaborated my master's thesis independently under supervision of Mgr. Kateřina Poláková, Ph.D. and all sources are included in the bibliography.

Olomouc: .....

Jan Belza

ACKNOWLEDGEMENT

I would first like to thank my supervisor Mgr. Kateřina Poláková, Ph.D. for valuable advices, opportunities and boundless patience. I would also like to thank my colleague Mgr. Tomáš Malina who helped me a lot with many experiments. Special thanks go to our leaders RNDr. Václav Ranc, Ph.D. and prof. RNDr. Radek Zbořil, Ph.D. for the opportunity to work in RCPTM. Many thanks go also to Aristides Bakandritsos, Ph.D. and Bc. Veronika Šedajová for providing me graphene acid and to all my colleagues from RCPTM, especially from the Bio-Med team.

Finally, I must express my very profound gratitude to my beloved wife Františka, to my parents and rest of my family for providing me with unfailing support and continuous encouragement during my studies, researching and writing this thesis. Thank you.

BIBLIOGRAFICKÁ IDENTIFIKACE

Autor: Bc. Jan Belza

Název práce: Experimentální studie interakcí buněk s nově vyvinutými deriváty grafenu

Typ práce: Diplomová práce

Vedoucí práce: Mgr. Kateřina Poláková, Ph.D.

Rok obhajoby: 2018

Pracoviště: Katedra fyzikální chemie a Regionální centrum pokročilých technologií a materiálů, Univerzita Palackého v Olomouci

Abstrakt: Grafen a jeho deriváty přitahují v posledním desetiletí obrovskou pozornost díky jejich možnému využití v biomedicíně, a to například jako materiálů pro biologické zobrazování, tkáňové inženýrství a doručování léků či genů. V této diplomové práci jsou shrnuty aktuální poznatky o biologických aplikacích grafenu a jeho derivátů. Dále je v této práci představen zcela nový hydrofilní derivát grafenu zvaný grafenová kyselina (G-COOH). Cílem této práce je zkoumání biologických interakcí G-COOH, stejně jako jejího případného využití v genové terapii jako vektoru pro doručování genů. V první řadě byla provedena systematická analýza cytotoxicity G-COOH, která potvrdila excelentní biokompatibilitu tohoto materiálu. Následně byla G-COOH povrchově modifikována kationickým polymerem polyethyleniminem. Výsledné konjugáty získaly schopnost vazby DNA a jsou tedy potenciálně využitelné v genové terapii.

Klíčová slova: grafen a jeho deriváty, grafen oxid, grafenová kyselina, cytotoxicita a bioaplikace grafenových nanomateriálů, povrchová modifikace polymerem, přenos genů, transfekce

Počet stran: 53

Jazyk: Angličtina

BIBLIOGRAPHIC IDENTIFICATION

Author: Bc. Jan Belza

Title: Experimental studies of interactions of cells with newly developed graphene derivatives

Type of thesis: Master's thesis

Supervisor: Mgr. Kateřina Poláková, Ph.D.

Department: Department of physical chemistry and Regional centre of advanced technologies and materials, Palacký University, Olomouc

Year of presentation: 2018

Abstract: Graphene and its derivatives have attracted enormous attention in the past decade due to their potential biological applications including bioimaging, tissue engineering and drug/gene delivery. In this master's thesis, the current knowledge on biological applications of graphene-based nanomaterials is summarized and newly developed hydrophilic graphene derivative called graphene acid (G-COOH) is presented. The goal is to explore biological interactions of G-COOH as well as possible application of graphene acid as a gene delivery vector. Firstly, a systematic study of G-COOH cytotoxicity was performed. These analyses confirmed its excellent biocompatibility. Secondly, graphene acid was conjugated with cationic polymer polyethyleneimine forming DNA-binding nanoparticles with possible application in gene therapy.

Key words: graphene and its derivatives, graphene oxide, graphene acid, cytotoxicity and bioapplications of graphene-based nanomaterials, polymer surface modification, gene transfer, transfection

Number of pages: 53

Language: English

LIST OF ABBREVIATIONS

Cy	cyanine (fluorescent dye)
Da	Dalton
DMEM	Dulbecco`s modified Eagle`s medium
DNA	deoxyribonucleic acid
EDC	1-ethyl-3-(3-dimethylaminopropyl)carbodiimide
EGFP	enhanced green fluorescent protein
FBS	fetal bovine serum
FITC	fluorescein isothiocyanate
G-COOH	graphene acid
GCN	cyanographene
GO	graphene oxide
MES	2-(*N*-morpholino)ethanesulfonic acid
nGO	nano graphene oxide
PBS	phosphate buffered saline
PEI	polyethyleneimine
PVDF	polyvinylidene fluoride
rGO	reduced graphene oxide
RNA	ribonucleic acid
RT	room temperature
Sulfo-NHS	*N*-hydroxysulfosuccinimide
TBS	tris buffered saline

CONTENTS

1 INTRODUCTION

Nanomaterials are defined as materials composed of particles with at least one dimension less than 100 *nm*. Those made of carbon can be divided into three major groups based on its dimensionality - 0D, 1D and 2D. Fullerenes, nanodiamonds and carbon dots (0D), carbon nanotubes, nanofibers and nanoribbons (1D) and graphene (2D) have attracted significant attention in last decades due to their unique mechanical, optical, electronic, thermal and chemical properties.[1] Therefore, some literature refers to the 21st century as the Carbon Age.[2] The properties stated above implicate broad range of applications in physics, chemistry, biology and medicine. Following paragraphs will be dedicated exclusively to graphene and its hydrophilic derivatives accenting biological and biomedical applications.

The flagship graphene-based nanomaterial for these purposes is graphene oxide (GO) with its intrinsic biocompatibility, low cost and scalable production, and facile functionalization. GO was successfully used in drug/gene delivery, cancer therapy, biosensing and bioimaging. Some of GO-based nanomaterials have shown antibacterial properties while others can be used as scaffolds for cell culture.[3]

Graphene acid, a newly developed graphene derivative will be presented in this thesis. In biology and biomedicine, graphene acid shares the application potential with GO, but remains unexplored. Its cytotoxicity profile will be compared to that of GO, as well as possible advantages over this well-established nanomaterial. As a first potential application, the use of graphene acid as a gene delivery vector was selected to explore.

1.1 Graphene

Nanomaterials form a separate universe halfway between molecules and bulk matter. One of the youngest shining stars among them is called graphene which is two-dimensional sp^2-hybridized carbon allotrope discovered by Andre Geim and Konstantin Novoselov in the year 2004.[4] The honeycomb structure of graphene is basic building block of many other carbon allotropes. Graphene can form graphite by stacking, nanotubes by rolling or fullerenes by wrapping of its sheets (Figure 1).[5]

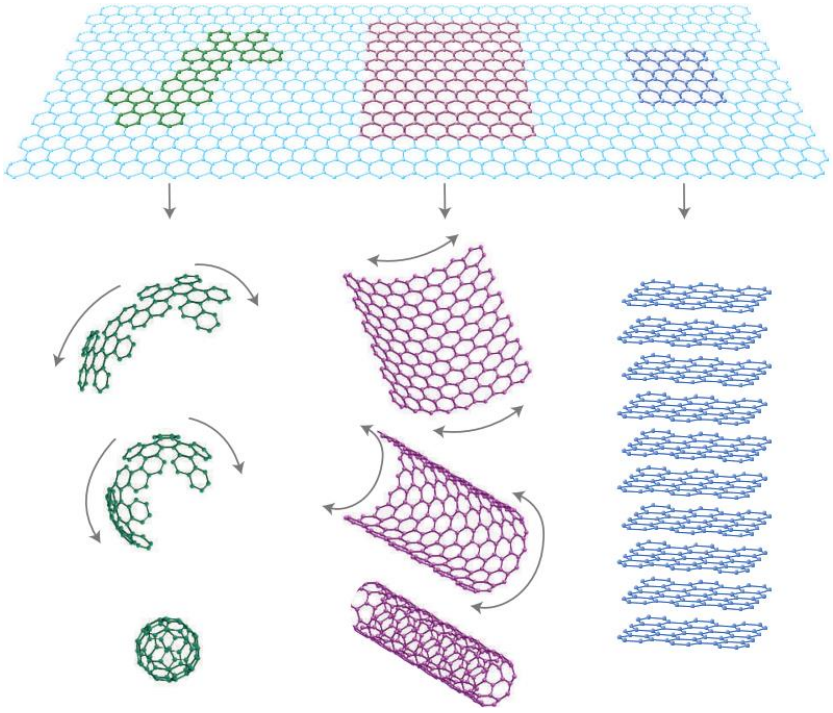

Figure 1: Graphene is a basic building block of other important carbon allotropes, adapted from ref. 5.

Due to graphene's unique properties, this atomically thin carbon layer has attracted a significant attention since its discovery. It has large theoretical specific surface area (2630 $m^2 \cdot g^{-1}$) and long-range π-conjugation in graphene yields exceptional electronic conductivity (intrinsic mobility of charge carriers 200,000 $cm^2 \cdot V^{-1} \cdot s^{-1}$). It has also high Young`s modulus (~1.1 *TPa*) and thermal conductivity of ~5000 $W \cdot m^{-1} \cdot K^{-1}$. [6]

The straightforward approach that led to the first isolation of single sheets of graphene (Figure 2) consisted in the peeling of graphite flake deposited on cellophane tape to successively remove layers from the sample. In this method, van der Waals interaction with the substrate can delaminate a single layer when the tape is peeled off the thick graphite flake. Although this method is simple in principle, it can be very

difficult to perform. But with practice, it can lead to high-quality graphene sheets with size more than 100 square μm.[6] Many other protocols of graphene preparation were subsequently developed using various methods including chemical vapour deposition (CVD),[7] silicon carbide (SiC) surface graphitisation,[8] methods employing mechanical exfoliation and other methods that use reductive reactions.[9]

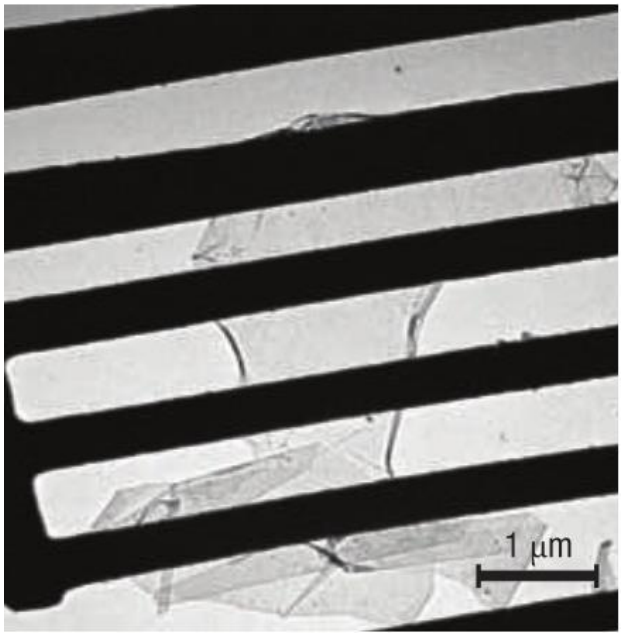

Figure 2: Bright-field TEM image of freely suspended graphene sheet. Adapted from ref. 10.

Graphitisation of SiC and CVD employing vacuum annealing are methods of choice to obtain large-scale production of graphene. As an example, David *et al.* synthesised graphene using CVD on Ni and Cu substrates within 30 minutes by rapid heating and quenching at atmospheric pressure and 70 minutes via slow heating and fast cooling of the substrate. However, these methods produce a mix of graphene monolayers and few-layered graphene which deteriorates the properties of the product. This happens due to the tendency of graphene monolayers to restack.[10] For example, the CVD on Ni film results in product that has approximately 1 to 12 graphene layers.[11] To obtain graphene monolayers, the interlayer distance has to be increased to 12 $\AA$ using physical or chemical approaches.[2]

Originally, it was thought that single graphene sheet cannot exist since perfect 2D crystals are thermodynamically unstable. However, freely suspended graphene monolayers are stable and show a long-range crystalline order. As published by

Meyer *et al.*, the transmission electron microscopy studies have revealed that suspended graphene sheets exhibit intrinsic microscopic roughening and are not perfectly planar. They discovered out-of-plane deformations reaching 1 *nm* and that the normal vector varies by several degrees which explains apparent graphene monolayer stability (Figure 3).[12]

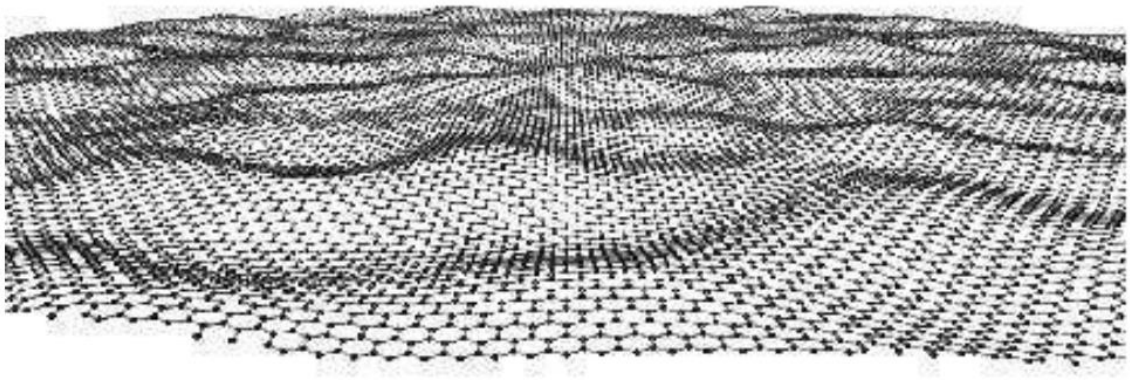

Figure 3: A theoretical model of graphene sheet that demonstrates out-of-plane deformations, adapted from ref. 18.

1.1.1 Graphene, its derivatives and biology

With the advances in methods of synthesis and functionalisation, graphene and its derivatives have shown great potential in energy technology (*e.g.* hydrogen storage, fuel cells, supercapacitors), sensors, catalysis, composite materials, nanoelectronics, environmental applications and recently, the biological and medical applications were brought into attention.[3]

Nanomedicine, among others, is one of the emerging branches of nanotechnology. There is an immense potential for use of graphene and graphene-related nanomaterials in detection of important biomolecules, diagnostics and treatment of various diseases, as in *in vitro* and *in vivo* bioimaging and gene transfection.[13] As an example, carbon nanotubes (CNTs) are already available for biological and medical purposes.[14] The suitability of graphene and its derivatives for biological and medical applications comes from their unique properties and biocompatibility. They exhibit fluorescence in VIS and NIR which leads to their use as biosensors and cell imaging agents. The mechanical properties of graphene make it useful in cell culture[15] and building self-supporting and structurally adaptive scaffolds.[16] As published by Podila *et al.*, graphene coating can also enhance the hemocompatibility of nitinol

stents.[17] Discovery of graphene led to the explosion in producing publications concerning graphene and its biologically and medically important derivatives *e. g.* ultrathin graphite, graphene nanosheets, few layer graphene, GO and reduced GO (rGO). These derivatives will be discussed in detail in the next chapter.

1.2 Oxidized graphite and graphene oxide

In the year 1859, professor Brodie from the University of Oxford published an article referring to a material named as graphic acid which was prepared from lamellar Ceylon graphite by repeated oxidation using potassium chlorate and fuming nitric acid.[18] Nowadays, it is known as graphite oxide and many other procedures of its preparation have been brought to the attention.

Exfoliated form of graphite oxide is known as graphene oxide (GO) which is chemically nearly identical to graphite oxide, but structurally it is very different (Figure 4). It can serve as a precursor for graphene synthesis but has interesting properties itself. GO contains distinct oxygen functional group that are responsible for its dispersability in water and possibility of further chemical derivatization.[19]

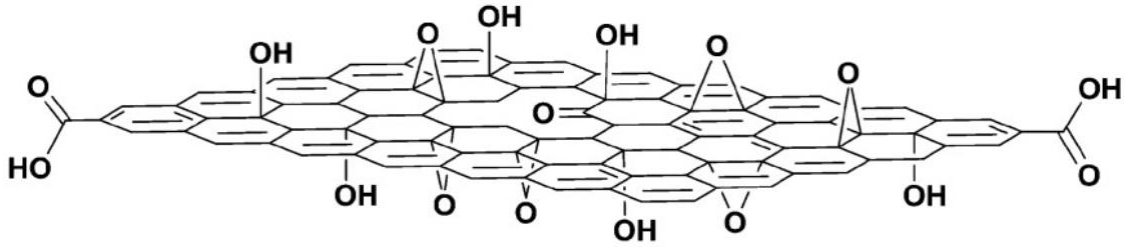

Figure 4: Schematic model of graphene oxide.[20]

1.2.1 Synthesis and structural properties

Graphite oxide is commonly prepared using top-down approaches by treating graphite with strong oxidizing agents (*e.g.* nitric acid or potassium permanganate).[18,21,22] Following exfoliation of graphite oxide results in production of GO nanosheets.[19] Successful exfoliation is achieved by low-power water bath sonication of graphite oxide aqueous dispersion in slightly basic conditions, which

stabilize the colloidal GO.[20] However, an environmentally friendly bottom-up synthesis of GO has been proposed by Tang L. *et al.*[23]

Preparation of graphite oxide and graphene oxide

The very first method of graphite oxide preparation invented by B. C. Brodie is performed by mixing a portion of graphite with excessive amount of potassium chlorate followed by addition of "sufficient" quantity of fuming nitric acid. This mixture is then heated at a temperature of 60 °C for three to four days and after drying, the oxidization step is repeated three times.[18] In 1898, the original Brodies' method was modified by L. Staundenmaier[22] who added $KClO_3$ in multiple aliquots during the reaction progress. In addition, he also used sulfuric acid to make the mixture more acidic. Staudenmaiers' method typically provides the most oxidized graphite oxide. Nevertheless, both Staudenmaiers' and Brodies' methods are time consuming and hazardous because of development of ClO_2, which is highly toxic and tends to decompose in air to produce explosions.[20]

A well-known method for graphite oxide preparation has been developed in 1957 by W. S. Hummers and R. E. Offeman.[21] Employing some modifications, this is the most widely used method since it is less time consuming and hazardous than the other procedures.[24] It consists in treating graphite flakes with concentrated sulfuric acid, sodium nitrate and potassium permanganate. The process is completed within two hours at temperatures below 45 °C. Resulting material has a carbon to oxygen ratio between 2.1 to 2.9 and a bright yellow colour when highly oxidized. For higher carbon to oxygen ratio, the colour is turning black.[21] The considerable drawback of the Hummers' method is potential contamination by permanganate ions. These ions have to be removed by treatment with hydrogen peroxide followed by washing and dialysis.[25] This method suffers from some other flaws, including generation of toxic NO_2 and N_2O_4, residual nitrate and low yield. Various modifications that have been made in the past 20 years address these problems. The main strategies lay in direct removal of $NaNO_3$ from Hummers' method with an improved workup; preoxidation before $KMnO_4$ oxidation in the absence of $NaNO_3$ (using $K_2S_2O_7$ and P_2O_5); increasing the amount of $KMnO_4$ instead of $NaNO_3$ and replacing $KMnO_4$ with K_2FeO_4 while nitrate was removed.[24]

Structural properties of graphite oxide

The most recognised model of graphite oxide is that published by Lerf and Klinowski.[26] Based on NMR studies, they proposed that graphite oxide contains C-OH groups and epoxide groups (1,2-ethers). The presence of terminal carboxyl groups has been proved by infrared spectroscopy. In the structure of graphite oxide, two kinds of regions are involved. One of them is aromatic region containing unoxidized benzene rings and the next is region with aliphatic six-membered rings (Figure 5). Aromatic entities, epoxide groups and double bonds form a nearly flat carbon grid. The carbons bonded to OH groups possess a slightly distorted tetrahedral configuration which gives raise to some wrinkling of the layers. The positions of functional groups are above and below the carbon layer.[26] Graphite oxide retains a stacked structure, whereas a chemically nearly identical GO is rather exfoliated into few-layered stacks or even monolayers.

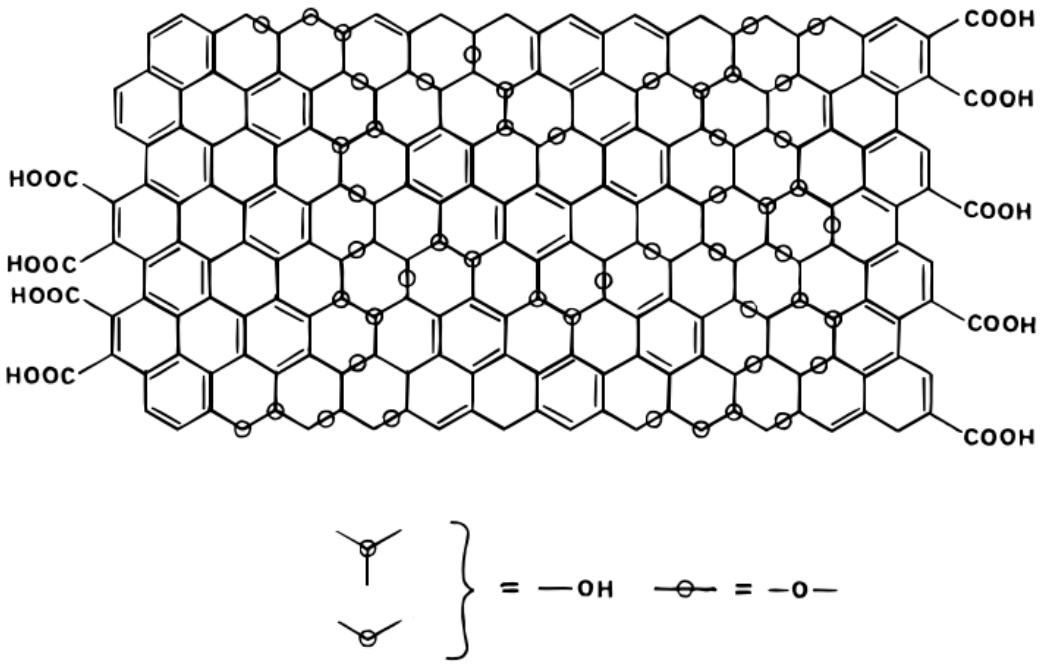

Figure 5: The Lerf-Klinowski model of graphite oxide.[26]

1.2.2 Biomedical applications

The reactivity of GO functional groups allows it to be covalently or non-covalently modified by biologically relevant molecules such as proteins, antibodies, peptides and nucleic acids. It has also been used for tissue engineering,[27] drug/gene delivery and bioimaging.[28]

Drug delivery

GO with its high surface area and ability to cross the cell membrane has great predispositions to be a carrier for drug delivery.[2] Most of the studies were focused on targeted delivery of anti-cancer drugs (*e.g.* camptothecin, doxorubicin, paclitaxel). To mention some examples, Dai *et al.*[29] used GO-PEG for loading of camptothecin (CPT) analogue, SN38 via π-π stacking. In this initial study, resulting material exhibited good solubility and high cytotoxicity. In another study, the anti-cancer drug paclitaxel was loaded onto GO-PEG in the same way.[30] Different delivery system was used by Jin *et al.*[31] They prepared hematin-conjugated dextran-functionalised GO (GO-HDex) which could efficiently bind doxorubicin (DOX). Moreover, the release of doxorubicin exhibits pH dependent profile. These and some other examples[32–34] are listed in Table 1.

Table 1: GO-based drug delivery systems.

Drug carrier	Drug delivered	Target	Ref.
GO-PEG	SN38	Human colon cancer cells HCT-116	29
GO-PEG	Paclitaxel	Human lung cancer cells A549	30
GO-HDex	DOX	Human MCF-7/ADR cells	31
GO-Folic acid	DOX + CPT	Human MCF-7 cells	32
GO-Chitosan	5-fluoroacil and ibuprofen	CEM cancer cells	34
GO	Hypocrellin A	HeLa cells	33

Bioimaging

Bioimaging plays essential roles in both research and clinical practice and allows the observation and study of biological processes from subcellular levels to small animals.[35] With the use of specific molecular probe or contrast agent, bioimaging enables us to detect diseases in its early stage and to monitor the treatment response.[36] The high surface area and versatile functionalisation of GO provides space for conjugation with small-molecular dyes, polymers, fluorescent nanoparticles, or biomolecules to obtain graphene derivatives ideal for bioimaging applications.[37] This part is mainly focused on the use of GO-derived nanomaterials for optical imaging in biological applications.

The use of intrinsic photoluminescence of nGO for fluorescence cell imaging was reported by Sun *et al.*[38] They found it to be photoluminescent in the near-infrared region with little background. In their experiments, pegylated nGO was loaded with doxorubicin via π-π stacking and functionalised with antibody for selective killing of cancer cells *in vitro*. However, the fluorescence of pegylated nGO has low quantum yield, which limits further *in vivo* applications. To overcome this issue, GO is functionalised with small-molecular dyes to enhance the fluorescence, thus enabling *in vitro* and *in vivo* imaging. As an example, Yang *et al.*[39] prepared a covalent conjugate of nGO-PEG with Cy7 dye for *in vivo* fluorescence imaging (Figure 6). They observed highly efficient passive tumour targeting in mice and utilised the NIR absorption of Cy7 for efficient photothermal therapy using low-power NIR laser.

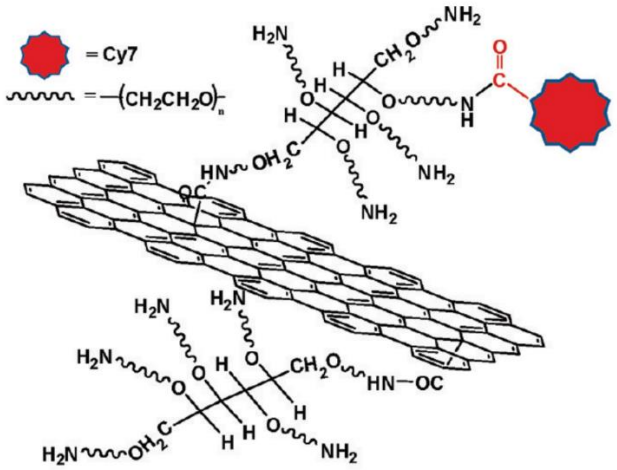

Figure 6: A covalent conjugate of pegylated GO with Cy7 dye for fluorescence imaging.[39]

Tissue engineering

Tissue engineering is a medical approach to repair, maintain, or improve the function of a tissue or whole organ. It uses a combination of appropriate cells, biochemical factors and scaffold material.[40] Developing suitable scaffold biomaterials is a key parameter. Desired biomaterials must mimic the biological environment and enable cell attachment, proliferation and differentiation by providing surfaces to interface with living cells. In addition, the biomaterials should be also support for new tissue formation. Other essential properties of such materials include biocompatibility, controlled biodegradability or bioresorbability by surrounding tissues to avoid necessity of surgical removal and high porosity to favour tissue integration and

vascularisation.[41] In this field GO has attracted significant attention due to its extraordinary mechanical strength, electrical conductivity, stiffness and facile functionalisation.[42,43] Therefore it can be used in various ways in tissue engineering. In addition GO has similar dimensions to those of extracellular matrix (ECM) components, so it can be considered as a physical analogue of ECM.[44] Possible applications of graphene family nanomaterials in tissue engineering are indicated in Figure 7.

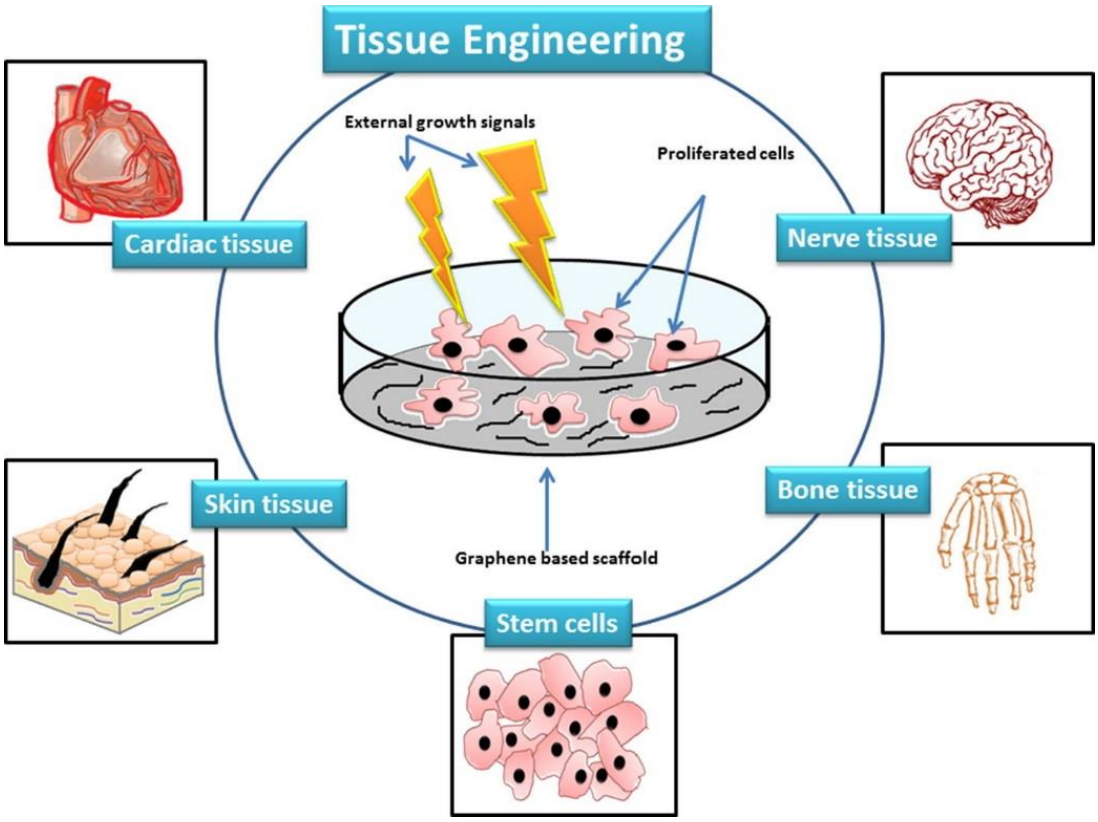

Figure 7: Possible applications of graphene family nanomaterials in tissue engineering.[45]

GO can serve as a reinforcement material in hydrogels, films, fibres, and other tissue engineering scaffolds enhancing their stability, mechanical properties, water retention, lubricity and can improve adhesion, differentiation and function of the cells.[16,27] As published by Cerruti *et al.*, a highly porous 3D GO/hyaluronic acid (GO/HA) hydrogel was prepared. It showed high electrical conductivity, excellent mechanical properties, and good biocompatibility to mesenchymal stem cells (MSCs). Therefore this material is an excellent candidate for bone tissue engineering applications.[46] It has

also been found that GO nanosheets improve mechanical properties of chitosan hydrogel and poly(acrylic acid)/gelatine hydrogel scaffolds.[47,48] Additionally, Park *et al.* presented a TWEEN/rGO hybrid "paper", a biocompatible material with high strength and antimicrobial activity.[49] They found it to be perfect candidate for several biomedical applications including stents, nail implants and strong invasive instruments.

In addition to mechanical improvement GO can be used for specific tissue engineering due to its electrical properties. Guo *et al.* presented a highly conductive poly(3,4-ethylenedioxythiopene) (PEDOT)-rGO hybrid microfiber.[50] They found that MSCs cultured on this hybrid microfiber exhibit enhanced proliferation and good neural differentiation tendency. Moreover, the neural differentiation of MSCs is rapidly improved by electric pulses generated by a self-powered triboelectric nanogenerator (TENG).

The possibility of surface modification of GO is also useful for tissue engineering applications. As reported by Gu *et al.*, the amine-functionalised GO shows excellent cell viability and proliferation with superior anticoagulation effects.[51] It also improved differentiation of cells into skeletal muscle due to adsorption of serum protein.[52] In another study, Lee *et al.* showed the adsorption of insulin on GO surface improving adipose tissue generation.[53] Additionally, GO coated with gelatine has been found to promote adhesion, proliferation, and osteogenic differentiation of MC3T3-E1 cells.[54] The same group observed similar results with carrageenan-functionalised GO.[55]

Gene delivery

Efficient and safe gene delivery vectors are essential for gene therapy which is a technique that uses genes to treat genetic diseases. This approach has attracted a lot of attention. The vector must protect the nucleic acid from degradation by nucleases and facilitate high transfection efficiency.[56] The high loading efficiency and increased gene transfection of graphene-based nanomaterials make them appropriate candidates for gene delivery. To obtain positive surface charge that is essential for electrostatic DNA binding properties they are tuned by surface modification with polymers, such as for example polyethyleneimine (PEI).[57] The pioneer work in this field was published by Feng *et al.*[58] They reported non-covalent GO-PEI nanosystem

capable of plasmid DNA binding and its subsequent delivery to HeLa cells with high transfection efficiency and no obvious toxicity. In another study, Kim *et al.* presented GO covalently modified with low-molecular weight branched polyethyleneimine. This nanoconstruct showed transfection efficiency as high as for high-molecular weight polyethyleneimine alone, but with significantly lower cytotoxicity. They also reported pohotoluminiscent properties of these particles and proposed it to be very promising agent in bioimaging and fluorescence-assisted cellular uptake tracking (Figure 8).[59] To enhance the transfection efficiency, Zhang and co-workers reported dual-polymer-functionalized GO. They covalently modified GO with polyethyleneimine and polyethylene glycol to obtain vector with transfection efficiency ~2.5-fold higher than that of widely used commercial transfection agents like Lipofectamine 2000 or bare PEI when used for transfection of hard-to-transfect cells such as Drosophila S2 cells.[60]

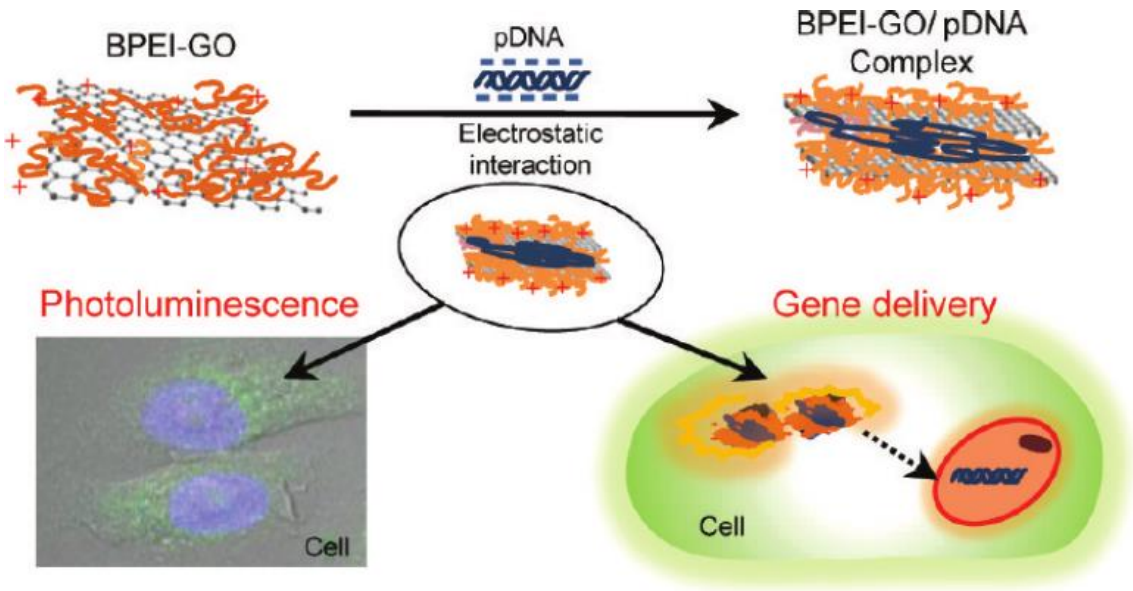

Figure 8: GO-polyethyleneimine nanoconstruct as a gene delivery vector and bioimaging tool.[59]

1.2.3 Interaction of graphene oxide with cells

Along with the application field expanding, the *in vitro* and *in vivo* safety of GO should be considered. The integral part of nanotoxicology research is assessing the biocompatibility of nanomaterials in tissue cultures and the cell-nanomaterial interaction in general. This is done by monitoring cellular uptake, subsequent biological effects and the fate of the nanomaterial in cells.[61]

Cellular uptake

When assessing the use of GO in biomedicine, its interaction with the surface of mammalian cells must be investigated. It is taken up into cells primarily via endocytic routes which can be divided into four categories: clathrin-mediated endocytosis, caveolae-mediated endocytosis, phagocytosis, and macropinocytosis. Uptake mechanism of GO has been observed to be cell type-dependent.[62,63] As an example, Linares *et al.* used eight specific inhibitors of endocytosis (chlorpromazine, colchicine, phenylarsine oxide, wortmannin, genistein, amiloride, cytochalasin D and cytochalasin B) to investigate the cellular uptake of GO by three different cell types (HepG2 hepatoma cells, RAW-264.7 macrophages and Saos-2 osteoblasts). As a result, macropinocytosis appears to be a general internalization process. Additionally, Saos-2 cells exhibit microtubule-dependent uptake of GO while RAW-264.7 and HepG2 cells employ clathrin-dependent pathways.[64]

The entrance of GO into cells is strongly influenced by its physicochemical properties such as size, shape, coating, charge, hydrodynamic diameter, isoelectric point, and pH gradient.[65] It has been found that large protein-coated GO nanosheets (~1 μm) are taken up primarily via phagocytosis and with decreasing size, clathrin-mediated endocytosis becomes the primary pathway. The interaction of graphene-based nanomaterials with the cell membrane is also dependent on its surface chemistry.[66,67] As published by Chatterjee, HepG2 cells can easily take up GO while reduced GO wraps cells leave around without internalization because of hydrophobic interaction with the cell surface.[68] Consequently prolonged exposure to high concentration of graphene induces physical and biological damage to the cell membrane, as well as destabilization of actin filaments and the cytoskeleton.[69] However even reduced GO flakes of different sizes can be internalized via endocytosis by certain types of cells.[70]

The dynamics of graphene materials internalization can be studied by both experimental and theoretical approaches. As an example, Li *et. al.* used coarse-grained molecular dynamics (MD) and all-atom MD to model the interactions between graphene and the lipid bilayer, as well as confocal and electron microscopy which showed its edge-first uptake and complete internalization.[69]

Cytotoxicity

As a follow-up to cellular uptake, cytotoxicity of nanomaterials is a crucial criterion when considering their possible biological applications. Chang and co-workers[71] have used single- or few-layered GO of three different sizes (780 nm, 430 nm and 160 nm, based on DLS) prepared from graphite powder by the modified Hummers' method to investigate it's *in vitro* toxicity on A549 cells. They analysed morphology of cells exposed to GO by optical microscopy and found that cells do not show any obvious difference between treated cells and control cells. In addition, no change in their adhesion to the culture dish was observed.

The cell viability was assayed by CCK-8 assay in which the formation of formazan dye depends on the mitochondria activity. They observed that the loss of viability is dose-dependent with the result that large- and medium-sized GO has a tiny influence on cell viability even at the concentration of 200 μg/mL. However, small-sized GO caused decrease of cell viability to 67 % at 24 hours after exposition at 200 μg/mL. Since nutrient depletion by nanomaterial can induce nanotoxicity, it was tested if the culture media pre-treated with GO have an influence on cell viability but no difference to control cells was observed. The cell mortality was analysed by Trypan blue exclusion assay in which the ratio of dead (blue) cells in all cells is estimated. This experiment revealed no significant change in cell mortality upon exposure to GO. The observed mortality ~1.5 % for treated cells and ~1.4 % for the control.

As mentioned earlier in this chapter, GO interacts with cell membrane. Therefore, the cell membrane integrity was monitored by the lactate-dehydrogenase (LDH) leakage. As a result, cells treated with GO had LDH leakage level around 6 % at a concentration of 200 μg/mL. This value was even lower than that of control cells in which the LDH leakage level was 7.5 %.

Autophagy

Autophagy is a catabolic pathway that maintains cell, tissue and organism homeostasis through degradation.[72] Increasing evidence suggests that the deregulation of autophagy may contribute to a broad spectrum of mammalian diseases.[73] It was reported that exposure of cell to certain nanomaterials, including carbon-based nanoparticles can elevate levels of autophagic flux. Therefore, there is an urgent need

for the study of possible health risks connected with autophagy.[74] Chen *et al.* published a study demonstrating that treatment of cells with GO triggers autophagy. It is likely that GO-triggered autophagy is exploited by the cells to clear the internalized GO.[75] In this thesis, a potential induction of autophagy by studied nanomaterial is monitored by the conversion of marker protein LC3B between its two forms (LC3B-I and LC3B-II).

1.3 Graphene acid

Graphene acid (G-COOH, Figure 9) is newly developed graphene derivative – a two-dimensional acid with the pK_A value of 5.2 and titration curve closely resembling that of molecular organic acids. G-COOH has many extraordinary properties such as, for example, high conductivity, biocompatibility and superior colloidal stability. As published by Bakandritsos *et al.*[76], graphene acid is prepared from fluorographene (FG) as a starting material since graphene itself is difficult to modify due to its low reactivity. As a first step, fluorographene is transformed into cyanographene (G-CN) that is fluorine-free and secondly, G-CN is hydrolysed to form G-COOH. The degree of functionalization reaches 13-15 % while its functionalization stays homogenous and selective which means that no other chemical groups are formed. Interestingly, G-COOH forms 3D supramolecular lattices upon drying. These lattices remind those formed by large polyaromatic hydrocarbon nanoflakes[77] which implicates well-defined structure and perfect colloidal properties of G-COOH. Additionally, presence of accessible carboxyl groups allows further conjugation of surface of G-COOH with various chemical moieties.

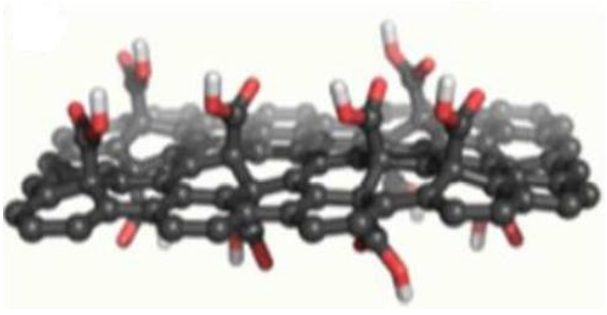

Figure 9: Schematic model of graphene acid, adapted from Bakandritsos *et al.*[76]

2 AIMS

The aims of this thesis are:

- to summarize a current knowledge on biological applications of graphene-based nanomaterials

- to explore biological behaviour of newly developed material called graphene acid and to test its biocompatibility

- to explore possible applications of graphene acid in gene delivery

3 MATERIALS AND METHODS

3.1 Physical material – graphene acid

Synthesis of G-COOH was performed according to the detailed protocol published by Bakandritsos *et al.*[76] Briefly, fluorinated graphene was sonicated in DMF, subsequently mixed with NaCN and heated yielding cyanographene (G-CN). Resulting material was separated by centrifugation and further purified by washing with DMF, dichloromethane, acetone, ethanol and water. To exchange sodium cations with H_3O^+, G-CN was washed with acidified water and suspended in fresh water after washing. Then HNO_3 (65%) was slowly added to the suspension to convert G-CN into G-COOH. The product was washed under acidic conditions. Following size selection was performed by repeated sonication (15 minutes, water bath sonicator) and centrifugation (1× 1,000g, 2× 2,000g) and the supernatant was collected. Finally, the pH was adjusted to ~8 forming stable aqueous suspension of graphene acid (see Figure 10 for TEM image). Synthesis and purification of G-COOH was performed by Dr. Aristides Bakandritsos and Bc. Veronika Šedajová (RCPTM).

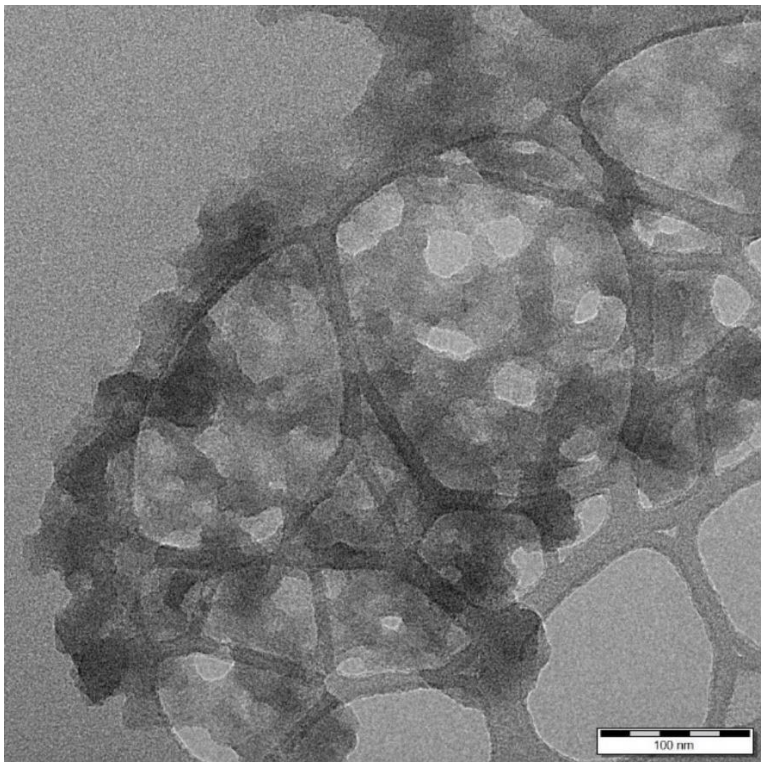

Figure 10: TEM image of final sample of G-COOH with the scale bar of 100 nm. This image was kindly provided by Bc. Veronika Šedajová.

3.2 Biological materials

For analyses of cytotoxicity of G-COOH healthy cells (mouse fibroblasts – NIH/3T3) and cancer cells (human cervical cancer cells – HeLa) were used.

3.3 Other materials and chemicals

Polyethyleneimine, branched, M_w 10,000 was purchased from Polysciences, Inc. (Warrington, PA), 1-ethyl-3-(3-dimethylaminopropyl)carbodiimide and graphene oxide were purchased from Sigma-Aldrich (Oakville, Canada). Plasmid DNA (pcDNA4_EGFP) was kindly provided to our laboratory by Dr. Jan Konvalinka.

3.4 List of instruments

Zetasizer Nano ZS (Malvern Instruments Ltd, UK)
Nicolet iS5 FTIR spectrometer (Thermo Scientific)
Fusion FX5 imaging system (Vilber-Lourmat)
BD FACSVerse flow cytometer (BD Biosciences)
Infinite M200PRO fluorescence reader (Tecan)
NB-203XL CO_2 incubator (N-Biotek)
IX70 fluorescence microscope (Olympus)
CKX31 microscope (Olympus)
Centrifuge 5430 R (Eppendorf)

3.5 Methods

3.5.1 Cell culture

In all experiments, NIH/3T3 and HeLa cells were cultured in DMEM media supplemented with 10% FBS in 5% CO_2 at 37 °C. For flow cytometry and ROS, cells were cultured in 96-well plates and in 6-well plates for autophagy analysis.

3.5.2 Flow cytometry analysis

Flow cytometry analyses were performed using BD FACSVerse flow cytometer (BD Biosciences) and commercial kits according to the manufacturer`s protocols. The kits used were: BD Annexin V FITC Apoptosis kit, BD Cycletest™ Plus DNA Reagent kit, MitoProbe™ JC-1 Assay kit (all BD Biosciences).

3.5.3 Dynamic light scattering and zeta potential measurement

DLS and Zeta potential measurements were performed using Zetasizer Nano ZS on appropriately concentrated aqueous dispersions of material of interest at defined pH value (see results section). Zeta potential was measured using disposable folded capillary cell DTS1070.

3.5.4 Fourier-transform infrared spectroscopy

FTIR spectra were recorded on a Nicolet iS5 FTIR spectrometer (Thermo Scientific) using Smart Orbit ZnSe ATR accessory. A droplet of an aqueous dispersion of material of interest was placed on the ZnSe crystal and left for water to dry and form a film. Spectra were then acquired by collecting 64 scans, using nitrogen gas flow through the ATR accessory. Baseline and ATR correction were applied to the collected spectra.

3.5.5 Monitoring of autophagic flux

Establishment of saturating concentration of chloroquine

HeLa cells were plated in 3 mL of DMEM per well in a six-well plate at a seeding density of 3×10^5. Cells were cultured for 48 hours to yield 90% - 100% confluency. At 48 hours after plating cells were treated with lysosomal inhibitor chloroquine diphosphate at concentrations varying from 5 μM to 50 μM and incubated for 6 hours. To harvest cells the medium was removed and the cells were rinsed three times with 1 mL of PBS, trypsinized with 200 μL of trypsin-EDTA for 3 minutes. Then 1 mL of DMEM was added and the cell suspension was collected in a 1.5-mL microcentrifuge tube. Cells were centrifuged at 1000×g for 5 minutes at room temperature and the medium was discarded. Cells were washed twice with 1 mL PBS, centrifuging under same conditions between washes. The PBS from the last wash was discarded and the cells were immediately flash-frozen in liquid nitrogen. Western blot analysis was then performed on obtained material detecting levels of LC3B-II to assess the saturating concentration of chloroquine diphosphate.

Treatment of cells in the presence and absence of chloroquine

HeLa cells were plated as described above. At 24 hours after plating cells were treated with two different concentrations of G-COOH ranging (5 $\mu g \cdot mL^{-1}$ and 100 $\mu g \cdot mL^{-1}$)

for additional 24 hours. Then chloroquine was added at its saturating concentrations (20 μM) to appropriate wells. Controls included cells incubated with chloroquine only, nanomaterial only and untreated cells. The cells were harvested and processed as described above.

Western blot analysis

Cells were lysed using RIPA lysis buffer with cOmplete™ Mini Protease Inhibitor Cocktail and incubated on ice for 1 hour. Lysates were then centrifuged at 20,000×g for 15 minutes at 4 °C and the supernatants were transferred into fresh microcentrifuge tubes. The protein concentration in lysates was quantitated using Bradford protein assay (Sigma-Aldrich) and samples were mixed with Laemmli sample buffer (1× final) and heated to 90 °C for 5 minutes in dry heating block. Resulting samples were loaded a ran on Tris-Glycine SDS-PAGE gel. The amount of total protein was 20 μg per well. Subsequently, proteins were transferred to a PVDF membrane (Millipore) using Mini Trans-Blot Cell (Bio-Rad) for 1 hour at 100 V. Membrane was blocked by incubating with Bløk-CH Noise Cancelling Reagent (Millipore). After 1 hour of blocking at room temperature antibodies against LC3B (Thermo) and β-actin (CST) were added and the membrane was incubated at 4 °C overnight. Next day the membrane was washed three times with TBST buffer for 5 minutes and subsequently incubated with HRP-conjugated secondary antibody diluted 1/10,000 in blocking buffer at room temperature. Membrane was then washed three times with TBST buffer as described above and incubated with Luminata Forte Western HRP substrate (Millipore). The chemiluminescence was detected using Vilber-Lourmat Fusion FX5 imaging system. Finally, densitometric analysis was performed using ImageJ software and the levels of LC3B-II were normalized to those of β-actin.

3.5.6 Conjugation of graphene acid with polyethyleneimine

Stock G-COOH dispersion – aqueous, 2.3 mg·mL^{-1}, pH 7.9 (adjusted with NaOH)

Graphene acid was sonicated in bath for 30 minutes and diluted with water to the concentration of 2 mg·mL^{-1}. After that, 100 μL of the G-COOH dispersion was mixed with 10 μL of branched PEI 10kDa (100 mg·mL^{-1}). The mixture was incubated

for 30 minutes on rotator. Then 100 μL of 0.1M MES pH 6.0 along with 2 mg of EDC was added to the mixture. Samples were then incubated overnight on rotator. Next day, the unreacted polymer was removed by washing three times with 1 mL of water. Samples were centrifuged for 30 minutes at 20,000×g between washing steps. Finally, the product was resuspended in 50 μL of water. After that, complexes with DNA were prepared by mixing 5 μL of G-COOH-PEI with 7 μg of DNA in 1 mL of water.

3.5.7 Conjugation of graphene oxide with polyethyleneimine

The protocol was the same as for G-COOH with the purification steps omitted due to instant precipitation of the product.

4 RESULTS

4.1 Optical microscopy of cells

The influence of graphene acid on cell morphology was analysed by phase contrast microscopy of NIH/3T3 cells after 24 h incubations with various concentrations of graphene acid. As a result, cells did not show any morphological changes in all concentrations used (figure 11).

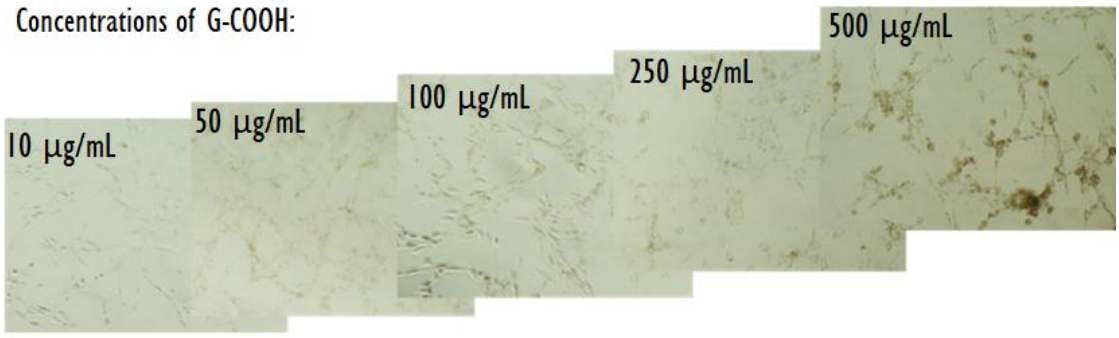

Figure 11: Optical microscopy images of NIH/3T3 cells after 24 h incubation with different concentrations (10 – 500 μg/mL) of G-COOH.

4.2 Reactive oxygen species (ROS) generation

Reactive oxygen species (ROS) generation and subsequent oxidation stress is one of the possible mechanism of cytotoxicity of carbon nanomaterials. Therefore, cells exposed to G-COOH were probed using CM-H_2DCFDA indicator, which detects various types of ROS, mainly hydrogen peroxide but also other radical species including hydroxyl, carbonate and thiyl radicals, as well as nitrogen dioxide.[78] The generation of ROS after 24 h incubation of NIH/3T3 and HeLa cells with various concentrations of G-COOH is indicated in the Figure 12. Low induction of ROS is observed in both cells lines.

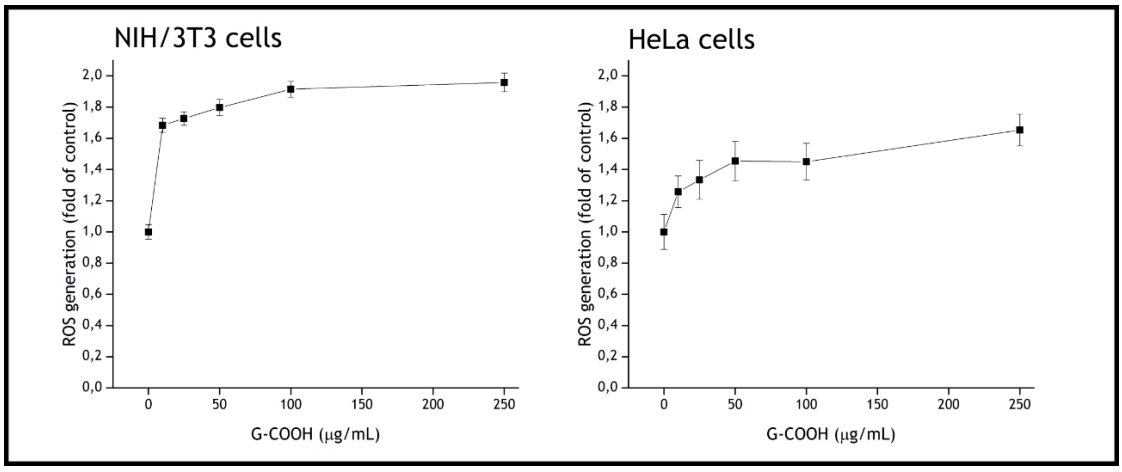

Figure 12: ROS generation in NIH/3T3 and HeLa cells after 24 h exposure to various concentrations of G-COOH ranging from 10 μg/mL to 250 μg/ml. Untreated cells were used as a control. Each error bar represents a mean statistical deviation of three independent experiments.

4.3 Flow cytometry analysis

4.3.1 Propidium iodide viability assay

Viability of NIH/3T3 and HeLa cells was measured using propidium iodide (PI) staining followed by flow cytometry analysis. Cells were exposed to various concentrations of G-COOH for 24 h. Resulting viabilities are depicted in Figure 13 for NIH/3T3 and HeLa cells respectively. The viability of both, NIH/3T3 and HeLa cells was not negatively affected by G-COOH. Even at highest concentration the viability stays >95 % when compared to control (untreated cells).

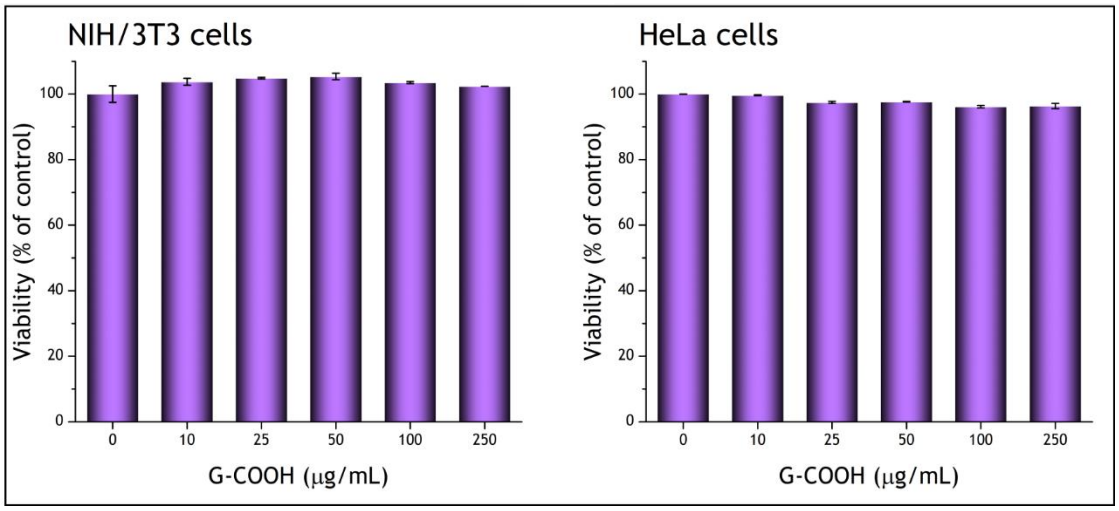

Figure 13: Viability of NIH/3T3 and HeLa cells after 24 h exposure to various concentrations of G-COOH. Each error bar represents a mean statistical deviation of three independent experiments.

4.3.2 FITC-Annexin V assay for apoptosis detection

To study apoptosis upon exposure to G-COOH cells were incubated with the same concentrations of G-COOH as in viability assay but for 4 hours only. After that, cells were stained with both PI and FITC-Annexin V antibody and analysed by flow cytometry. Three populations of cells were observed – unstained (alive), FITC positive (early apoptosis) and both FITC and PI positive (late apoptosis or dead). Only a little influence of G-COOH on both NIH/3T3 and HeLa cells is observed, indicating that G-COOH does not induce apoptosis under these experimental conditions (Figure 14).

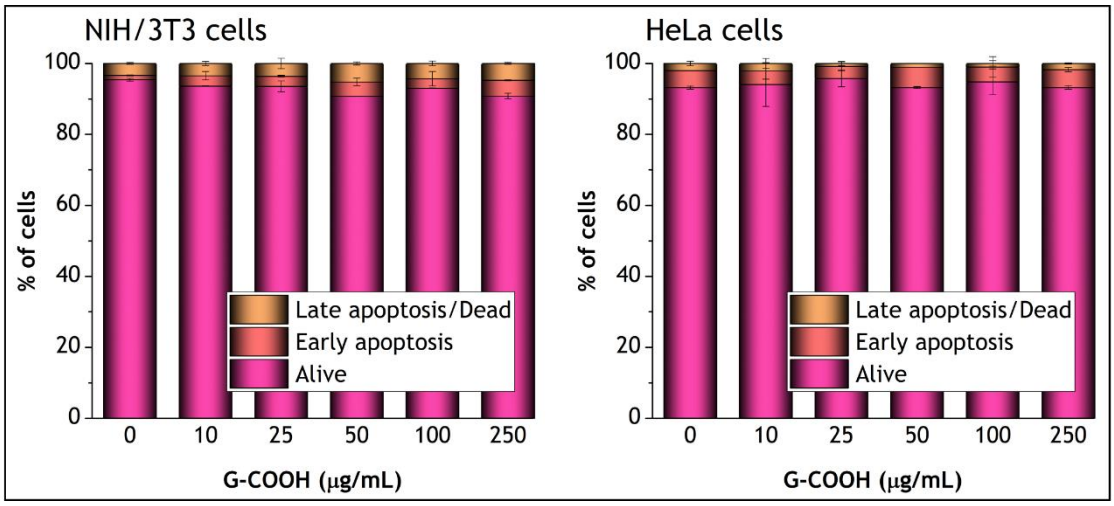

Figure 14: Influence of G-COOH on apoptosis induction after 4 h incubation using various concentrations of G-COOH. Each error bar represents a mean statistical deviation of three independent experiments.

4.3.3 Cell cycle analysis

The impact of various concentrations of G-COOH on the cell cycle was studied by flow cytometry after 24 h incubation. From the results of cell cycle analysis, we can suggest among others the influence on cell proliferation. In the case of G-COOH the impact on cell cycle was mostly insignificant (Figure 15). Only a small increase of G0/G1 in NIH/3T3 cells at highest concentration of G-COOH was observed, which indicates slightly lower proliferation.

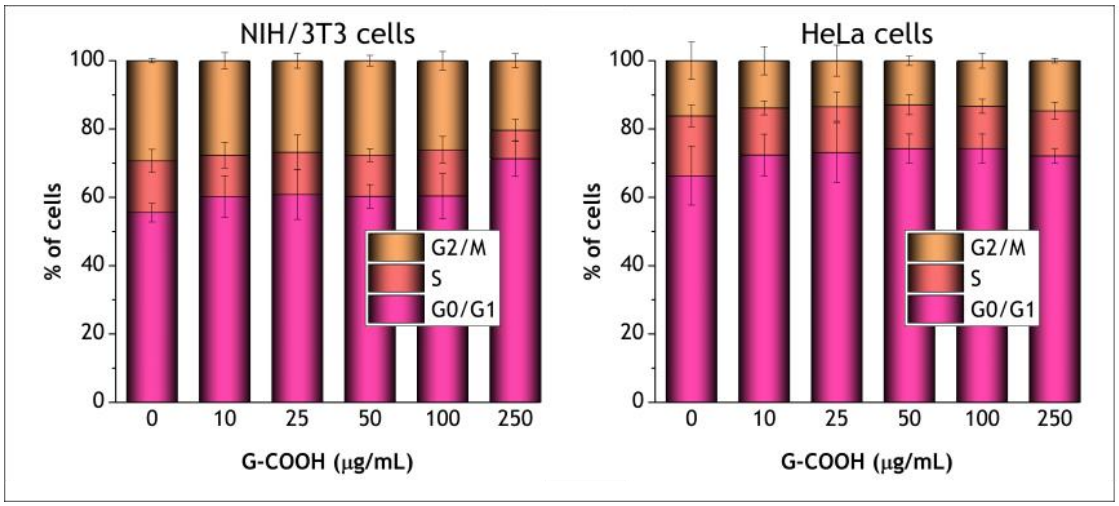

Figure 15: Cell cycle analysis of NIH/3T3 and HeLa cells after 24 h incubation with indicated concentrations of G-COOH. Each error bar represents a mean statistical deviation of three independent experiments.

4.3.4 Mitochondrial membrane potential

Mitochondrial membrane potential of NIH/3T3 and HeLa cells after exposure to G-COOH was studied by staining of cells with cationic dye JC-1 that is accumulated in mitochondria in potential-dependent manner. When analysed by flow cytometry two populations of cells are observed, those with intact inner mitochondrial membrane (red fluorescence) and those with damaged inner mitochondrial membrane (green fluorescence). In the graphs (Figure 16), decrease in treated cells with intact membrane compared to control cells is observed. In chosen concentration range, the MMP loss is insignificant for both, NIH/3T3 and HeLa cells.

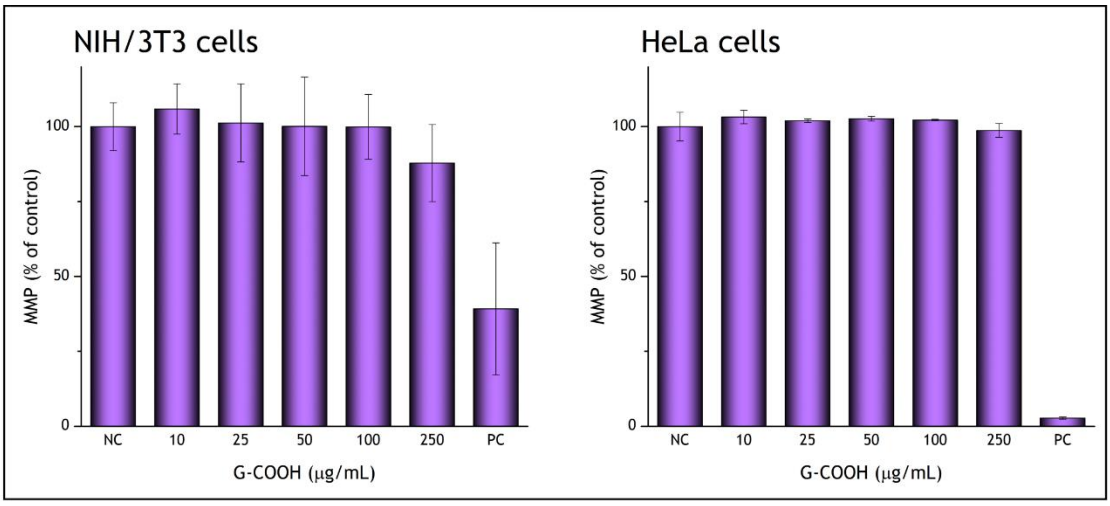

Figure 16: Analysis of MMP loss in cells exposed to various concentrations of G-COOH. Cells incubated with carbonyl cyanide 3-chlorophenylhydrazone were used as positive control (PC). Each error bar represents a mean statistical deviation of three independent experiments.

4.4 Monitoring of autophagic flux upon G-COOH exposure

Autophagy is a cellular pathway that can be induced by a nanomaterial. In this work it was studied by monitoring autophagy marker protein LC3 and its conversion between LC3-I and LC3-II. Western blot analysis was used to monitor this conversion and the LC3-II level was normalized against β-actin. HeLa cells were used for this experiment.

The so called LC3 turnover assay employs chloroquine (CQ), which is inhibitor of late autophagy where the autophagosome fuses with lysosome forming autolysosome. As a first step the saturating concentration of CQ is established and then the cells are treated with nanomaterial of interest in the presence and absence of CQ and the relative enrichment of LC3-II is studied.

4.4.1 Establishing the saturating concentration of chloroquine

The use of lysosomal inhibitor chloroquine (CQ) is important to prevent LC3B-II degradation during cell treatment by G-COOH and detecting autophagy. Therefore, a saturating concentration of CQ must be estimated. For HeLa cells, it was estimated to 20 μM by western blot. An image of the membrane was taken and analysed using densitometry (Figure 17).

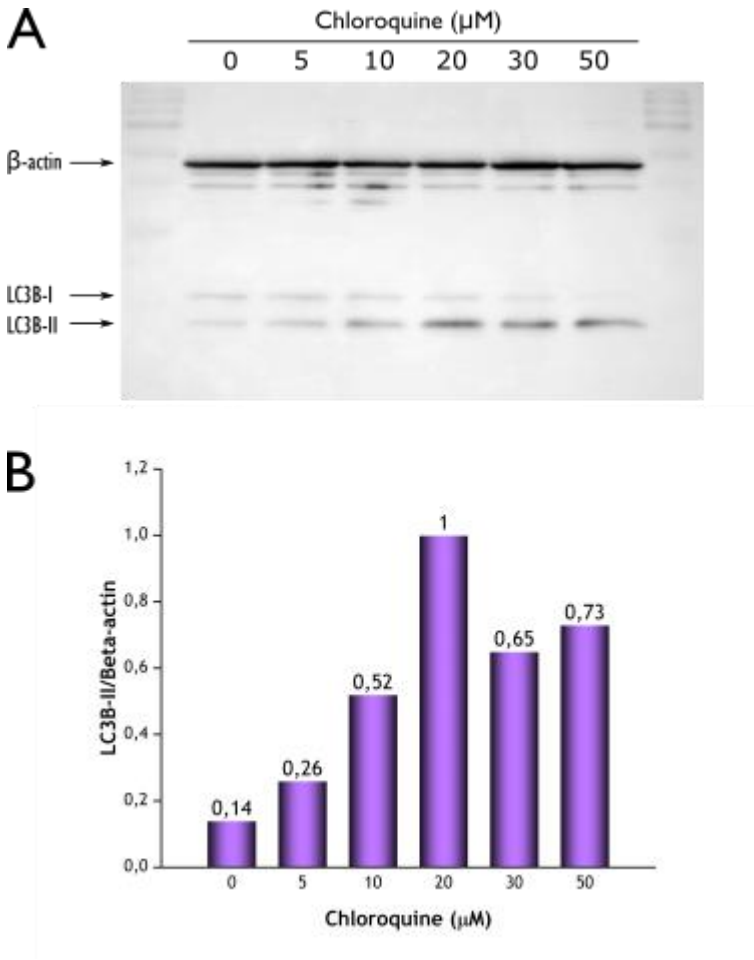

Figure 17: Establishing the saturating concentration for lysosomal inhibitor chloroquine (CQ) in HeLa cells. (A) Western blot analysis of the levels of LC3B-II in HeLa cells. Cells were seeded and cultured for 48 hours. After that, they were treated with increasing concentrations of CQ and incubated for 2 hours before harvesting. Western blotting was performed as described in method section. A home-keeping protein β-actin was used as a loading control. (B) Intensity of LC3B-II band was normalised against β-actin using ImageJ software. In HeLa cells, increase of the LC3B-II to β-actin ratio was observed up to the concentration of 20 μM. For higher CQ concentrations, the LC3B-II to β-actin ratio decreased. The saturating concentration of CQ was estimated to be 20 μM.

4.4.2 Autophagy induction by G-COOH

Two identical experiments showed that the induction of autophagy by G-COOH is concentration dependent. (Figure 18). Relative intensities of LC3B-II bands in the cells treated with G-COOH were compared to that of control cells. While the treatment with 5 $\mu g \cdot mL^{-1}$ G-COOH did not cause any difference, the higher concentration (100 $\mu g \cdot mL^{-1}$) increased autophagic flux when compared to control.

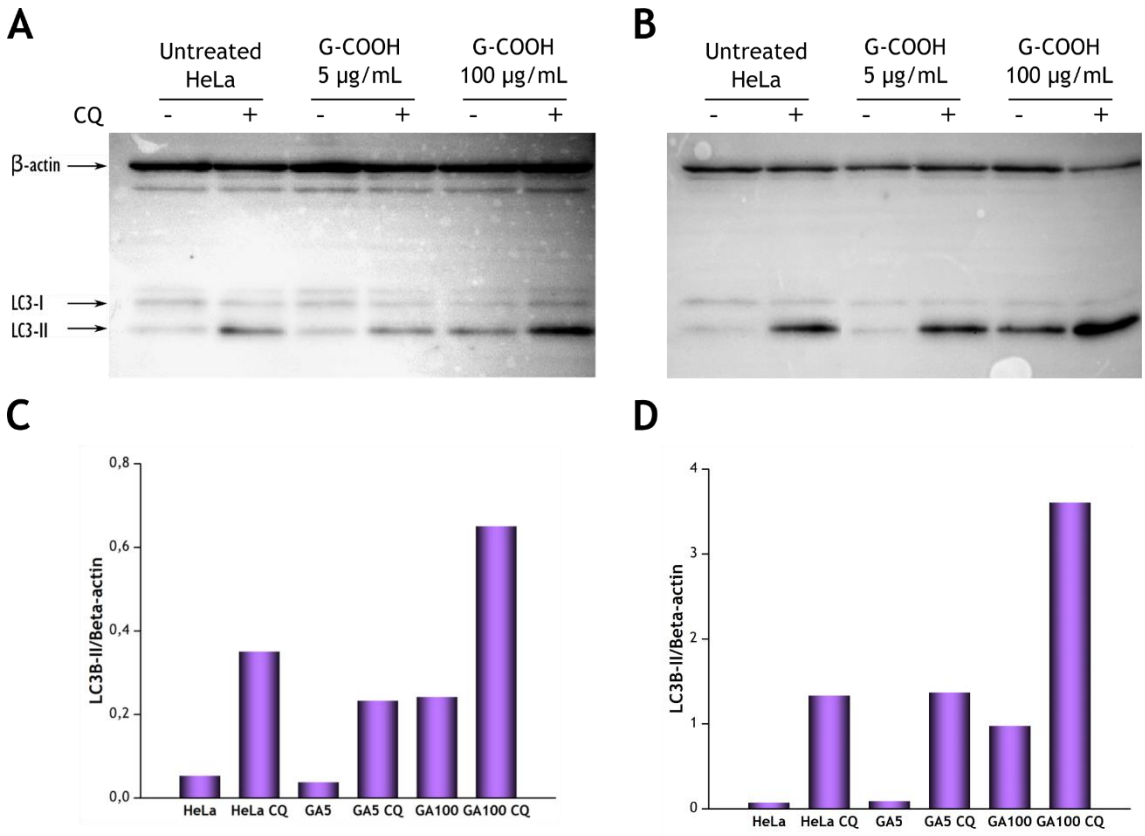

Figure 18: HeLa cells show concentration-dependent increase of autophagic flux when exposed to G-COOH. (A, B) Two identical western blot analyses were performed to explore the influence of two concentrations (5 µg/ml and 100 µg/ml) of G-COOH on autophagic flux. After 24 h treatment with G-COOH, the saturating concentration (20 µM) of CQ was added for additional 2 h before harvesting the cells. Untreated cells were used as a control. (C, D) Densitometric analysis of previous two western blots using ImageJ software represented by bar graphs displaying the LC3B-II/β-actin ratio. When exposed to 5 µg/ml G-COOH, the cells show autophagic flux level comparable to that of control cells. The G-COOH at a concentration of 100 µg/ml causes significant increase of autophagic flux in the cells.

4.5 Functionalisation of G-COOH for bioapplications

The experimental design consists of covalent functionalization of G-COOH with cationic polymer – polyethyleneimine (PEI). Resulting nanoparticles gain the ability to bind DNA via electrostatic forces and so they are potentially applicable as gene delivery vector (Figure 19).

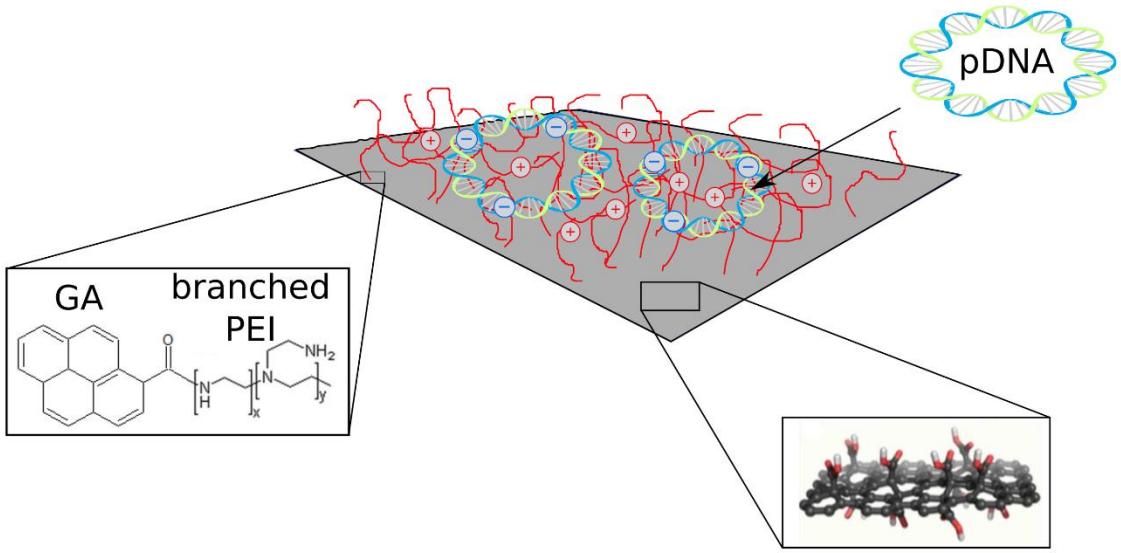

Figure 19: Illustration of G-COOH-PEI covalent conjugate with electrostatically bound plasmid DNA.

4.5.1 Size and stability

The photographs of reaction mixtures after overnight incubation indicate perfect colloidal properties of G-COOH-PEI (Figure 20). For comparison, analogous reaction with GO is shown. GO exhibited irreversible aggregation, which is in contradiction with literature.[58] The synthesis of GO-based gene delivery vector was not successfully reproduced by our laboratory.

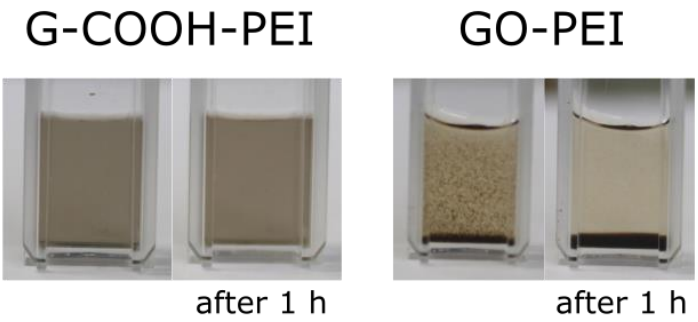

Figure 20: Comparison of stabilities of G-COOH-PEI and GO-PEI conjugates in water.

Three different sizes of branched polyethyleneimine were conjugated with G-COOH. The use of 800 Da PEI led to instant precipitation, the other two PEIs were 10 kDa and 25 kDa. The size and time stability of purified G-COOH-PEI10kDa and G-COOH-PEI25kDa in water were tested by DLS (Figures 21 and 22). The Z-average size is ~200 nm and does not change after 30 days of storage at 4 °C. These findings indicate superb colloidal stability of both G-COOH-PEI conjugates. For further

experiments, 10 kDa PEI was used due to its known lower cytotoxicity. After coating with PEI, the zeta-potential of G-COOH (~ -32 mV) rapidly increases to ~ +30 mV at pH 6.0 (data not shown).

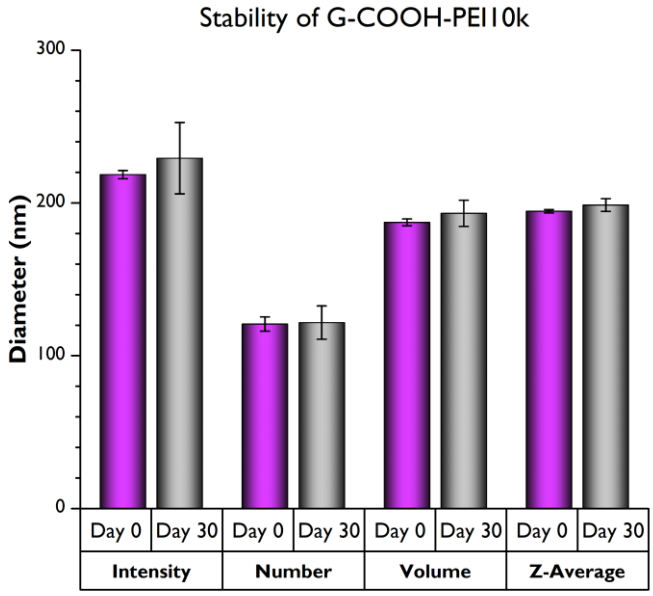

Figure 21: Stability of G-COOH-PEI10kDa conjugates immediately after synthesis and 30 days after synthesis measured by DLS.

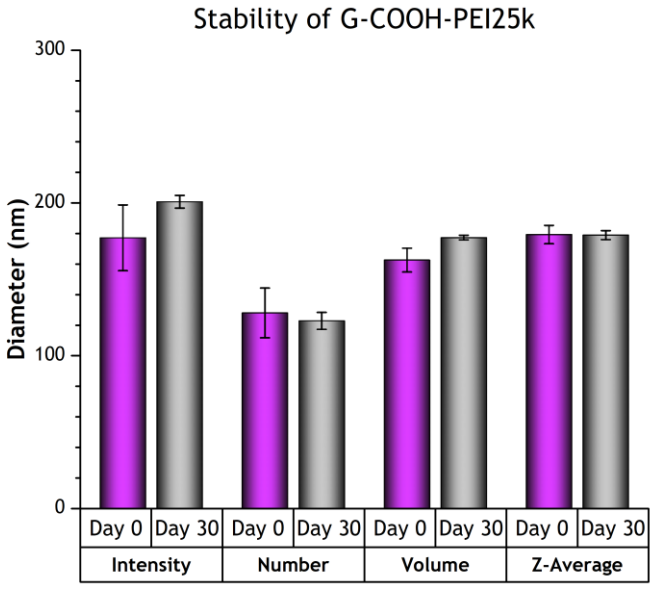

Figure 22: Stability of G-COOH-PEI25kDa conjugates immediately after synthesis and 30 days after synthesis measured by DLS.

4.5.2 FTIR analysis

FTIR analysis of G-COOH-PEI was performed to confirm successful conjugation of PEI (Figure 23). The spectrum of G-COOH-PEI (c) shows peaks characteristic for sp^3 C-H stretches of PEI (2800 – 3000 cm^{-1}) and the peak characteristic for carboxyl group of G-COOH (1730 cm^{-1}). These results confirm successful conjugation of G-COOH with PEI. For comparison, the spectra of PEI (a) and bare G-COOH (b) are showed. Even though the binding of PEI is apparent, it stays unclear if it is successfully bound by covalent bond or if it stays connected with G-COOH via electrostatic interaction.

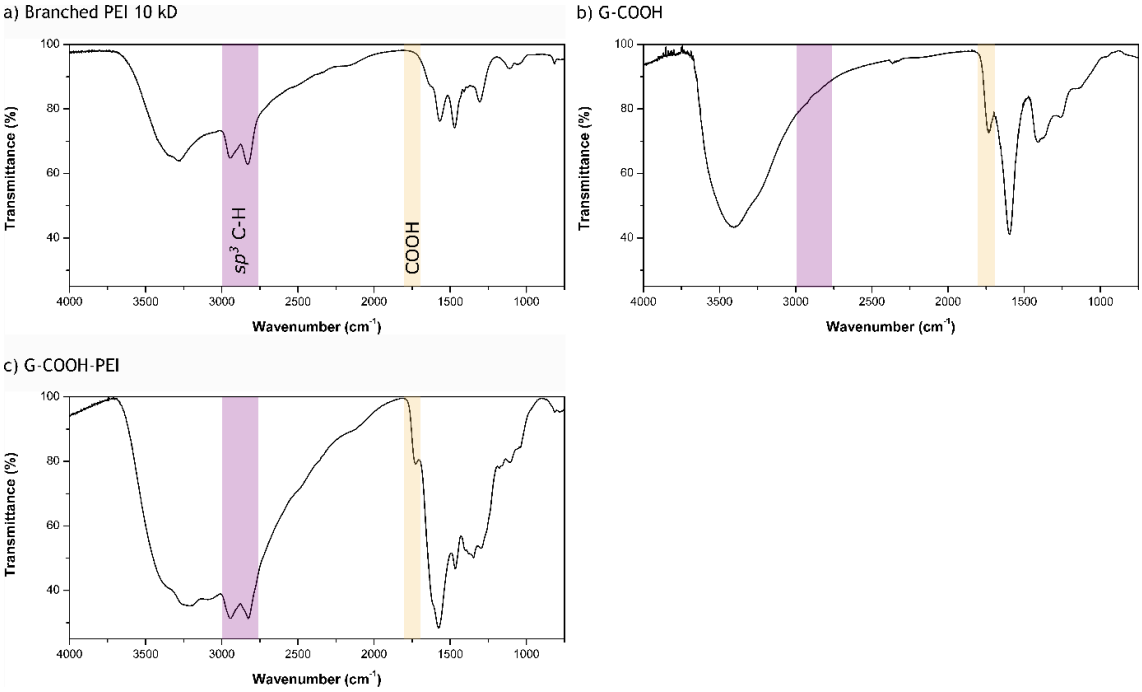

Figure 23: FT-IR spectra of branched PEI 10 kD (a), bare G-COOH (b) and G-COOH-PEI (c).

4.5.3 Characterisation of G-COOH-PEI/DNA complexes

The complexes of G-COOH-PEI and DNA were prepared simply by mixing it in water environment. This mixture was then incubated for 30 minutes. Resulting material was characterised by XPS (Table 2), which showed the presence of phosphorus in the sample of purified G-COOH-PEI/DNA, thus confirming DNA binding. The DNA binding capability of G-COOH-PEI was further characterised by UV spectroscopy (Figure 24). G-COOH-PEI/DNA complexes were centrifuged to pellet the nanoparticles and the UV spectrum of supernatant was measured.

As a result, the DNA peak (λ_{max} = 260 nm) was undetectable in the supernatant, while the DNA alone stays in solution. This experiment confirms binding of DNA independently on XPS. Since a lot of material is lost during purification steps, the DNA binding capacity of G-COOH-PEI remains unknown and should be further studied.

Table 2: XPS analysis of G-COOH-PEI and G-COOH-PEI/DNA complexes. G-COOH-PEI was mixed with DNA, washed by repeated centrifugation and analysed by XPS. The presence of phosphorus in the sample indicates successful DNA binding.

	CARBON (%)	NITROGEN (%)	OXYGEN (%)	PHOSPHORUS (%)
G-COOH-PEI	66.07	18.19	15.75	0
G-COOH-PEI/DNA	58.47	12.57	28.50	0.45

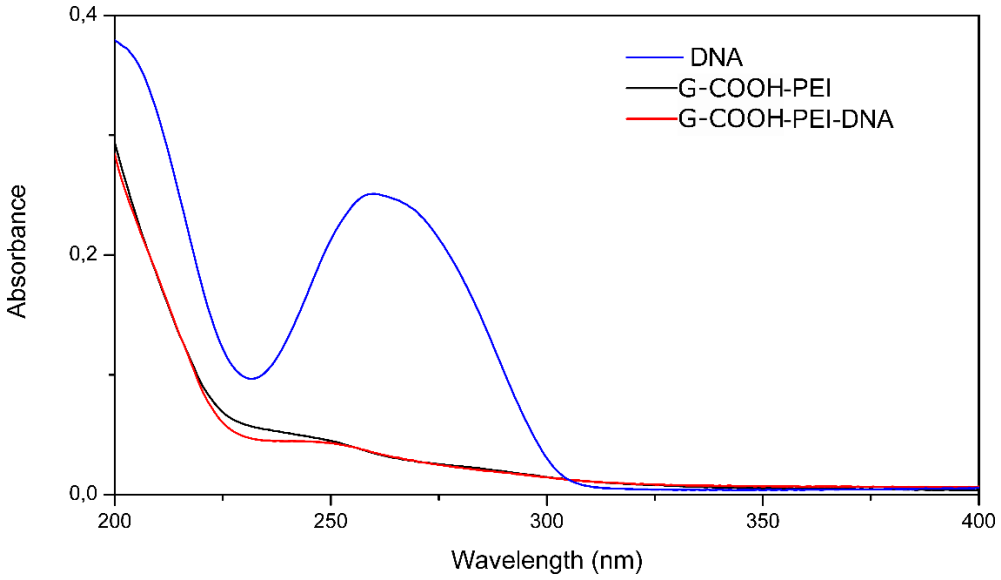

Figure 24: Ultraviolet absorption spectra of supernatants of DNA (blue), G-COOH-PEI (black) and G-COOH-PEI-DNA complexes (red). The ability of G-COOH-PEI to bind DNA is indicated by disappearing of absorption peak in supernatant at a wavelength of 260 nm after pelleting the nanoparticles by centrifugation.

5 DISCUSSION

This master's thesis is focused on newly developed hydrophilic graphene derivative – graphene acid (G-COOH). As suggested by the name, it is two-dimensional carboxylic acid with broad range of potential applications comparable to that of well-established graphene oxide. It can be chemically modified to customize its properties to make them suitable for desired application. In this thesis, biological interactions and potential biological applications of G-COOH were studied. For every biological usage of a nanomaterial, it is necessary to evaluate its potential health risks. Here, this was done by comprehensive *in vitro* toxicological study of potential unwanted effects of G-COOH on mammalian cells. Then, inspired by recent studies on GO, G-COOH was subjected to investigation of its potential usage as a gene delivery vector, which is urgently needed for the technique known as gene therapy.

The toxicity and biocompatibility of G-COOH was systematically studied on two different cell lines representing both, healthy and cancer cells. Mouse fibroblasts NIH/3T3, a widely used model cell line for toxicological studies, were selected to represent healthy cells and human cervical cancer cells HeLa were chosen as the second cell line. Recently, a less sophisticated cytotoxicity study on G-COOH was reported as a part of paper published by Bakandritsos *et al.* with satisfying results.[76] However, in that study the sample of G-COOH was not size-selected, which could have great impact on the cytotoxicity. As collectively indicated by the results reported in this thesis, G-COOH shows excellent biocompatibility to both, HeLa and NIH/3T3 cells up to 250 μg/mL. When compared to GO, G-COOH shows similar or better behaviour in the cell environment. A study performed by Chang *et al.* shows pretty good biocompatibility of GO to A549 cells up to 200 μg/mL.[71] In contrary, another study by Wang *et al.* shows significant toxicity of GO to human fibroblast cells at concentrations above 50 μg/mL.[79] This inconsistency may be caused by several factors, mainly by differences in the process of GO synthesis and by the fact that cytotoxicity is cell line-dependent. Based on these findings, G-COOH can be considered as a nanomaterial having lower cytotoxicity and better biocompatibility than GO. In the concentration range tested, G-COOH has no valuable impact on cell morphology, viability, apoptosis induction, cell cycle and mitochondrial membrane

potential (Figures 11, 13, 14, 15 and 16, respectively). Consistently with the study performed by Bakandritsos and co-workers, exposure of studied cells to G-COOH leads to very low increase in ROS generation (~1.9-fold for NIH/3T3 cells and ~1.6-fold for HeLa cells at 250 μg/mL of G-COOH, see Figure 12). Since oxidative stress is a well-recognized toxicological mechanism of various nanoparticles[80] and cells exposed to GO show significantly higher increase in ROS generation than that exposed to G-COOH,[71] these results are satisfactory. It was reported by Chen *et al.,*[75] that GO induces autophagy at concentrations as low as 5 μg/mL and causes significant cell death at 100 μg/mL. Therefore, we decided to investigate if this phenomenon is connected also with G-COOH. We found out that G-COOH does not elevate autophagy above its basal level at concentration of 5 μg/mL (Figure 18). At 100 μg/mL of G-COOH, autophagy was significantly induced but as indicated by previous results, no toxic effects were observed. These finding leads us to the hypothesis, that cells employ autophagy as mechanism of clearance of G-COOH. To summarize this part, G-COOH is perfectly biocompatible nanomaterial with possible advantages over GO in potential biological applications.

The goal of the second part of this master's thesis is to explore potential biological applications of G-COOH. Motivated by recent studies on GO,[59,81] we decided to investigate the possible usage of G-COOH as a vector for gene therapy. Our strategy was to covalently modify the surface of G-COOH with cationic polymer polyethyleneimine (PEI). This gave rise to high positive surface charge and leaded to DNA-binding capabilities of resulting nanoparticles (Figure 19). We decided to use branched PEI and started with four different molecular weights of PEI, 800 Da, 1.2 kDa, 10 kDa and 25 kDa. Branched PEI possesses many primary amine groups, while linear PEI has only terminal primary amines. Since our approach was covalent modification of G-COOH via reaction of primary amines of PEI with carboxyl groups of G-COOH, it was advantageous to use branched polymer. The molecular weight of polymer has significant impact on the properties of final nanoparticles. Low molecular weight PEIs are known to be less toxic and less effective in transfection and *vice versa*. We found out that the molecular weight of PEI also affects stability of resulting conjugates. The conjugation of G-COOH with 800 Da and 1.2 kDa

branched PEI leaded to instant aggregation of the sample, therefore, we omitted these polymers in further experiments. We prepared conjugates of G-COOH with 10 kDa PEI and 25 kDa PEI and studied their colloidal stability with DLS. As we found out, both samples were stable for long period at 4 °C (Figures 21 and 22). Based on these results, we picked G-COOH conjugated with 10 kDa PEI as the nanomaterial of interest. We expected 10 kDa PEI to be less toxic while retaining acceptable transfection efficiency (results not shown in this thesis). As referred by Kim *et al.*,[59] the transfection efficiency of conjugates should be further enhanced when compared to that of bare PEI. The conjugation of G-COOH with 10 kDa PEI was verified by FTIR spectroscopy. However, it remains unclear if the conjugates are strictly covalent or just electrostatic. It is likely that the binding mode of PEI to G-COOH represents a mix of covalent amide bond and electrostatic attraction. But importantly, the PEI was present on the surface of G-COOH and the conjugates showed long-term stability in water environment. After that, we performed successful DNA-binding trials with G-COOH-PEI10kDa conjugates. This was confirmed directly by XPS and indirectly by UV spectroscopy. Logically, the next step is cell transfection. Therefore, the strategy was to use plasmid DNA that bares gene for green fluorescent protein (GFP) and use the GFP fluorescence as a proof of expression of transfected DNA. We successfully transfected HeLa cells with this plasmid using bare 10 kDa PEI and observed all its disadvantages – low transfection efficiency and high toxicity of bare PEI. However, we have verified that the DNA is intact and ready to use for transfection of HeLa cells. But still, we were not able to efficiently transfect HeLa cells using G-COOH-PEI10kDa conjugates. These conjugates complexed with DNA rapidly aggregated in the medium containing fetal bovine serum and were not able to penetrate the cell membrane. As a control, we tried to reproduce previous studies made on GO[59,81] but without success. We observed irreversible aggregation of commercially available GO nanocolloids when exposed to all listed polymers, an example is shown in Figure 20. We also tried in-house prepared nGO for the conjugation with similar results. Inconsistently with literature, we were not able to synthesize GO-PEI conjugates, while the synthesis of G-COOH-PEI is relatively non-problematic. The drawback of our synthesis of G-COOH-PEI lays in the purification step where we are losing a significant quantity of nanoparticles during

the centrifugation. Our next plan is to purify the nanoparticles that are present in the supernatant rather than the pellet. The pelleted fraction is likely susceptible to aggregation, which could be the reason of aggregation of G-COOH-PEI/DNA complexes in cell environment. The purification of G-COOH-PEI conjugates from supernatant will be performed using gel permeation chromatography. The stability could be further improved by surface modification of G-COOH with PEI combined with polyethylene glycol (PEG). Polyethylene glycol is frequently used to coat nanoparticles to enhance their colloidal properties.[60] Finally, these approaches could help us to overcome the issues with stability of conjugates in serum-containing medium and could lead to successful gene transfection.

6 CONCLUSIONS

In conclusion, biological behaviour of new graphene-based nanomaterial called graphene acid (G-COOH) was reported. We observed superb colloidal stability which predicts a further chemical derivatization towards biological applications. Moreover, cytotoxicity results showed excellent biocompatibility in all studied concentrations (till 250 μg/ml) based on various cytotoxicity tests such as viability assay, analysis of induction of apoptotic pathway, analysis of cell cycle and study of mitochondrial membrane potential; all established for two different cell lines (NIH/3T3 and HeLa). Nevertheless, in high concentrations G-COOH induced autophagy in HeLa cells. However, in concentration relevant for biological applications the autophagy level is comparable to that of control untreated cells. Furthermore, a potential gene delivery vector based on graphene acid chemically-functionalised with cationic polymer polyethyleneimine (G-COOH-PEI) was reported. Due to its net positive charge density, it showed a strong ability to efficiently condensate plasmid DNA. This makes G-COOH-PEI a potential candidate for usage as a gene delivery vector.

7 REFERENCES

1. Choudhary, N., Hwang, S. & Choi, W. Carbon Nanomaterials: A Review. in *Handbook of Nanomaterials Properties* 709–769 (2014).

2. Tonelli, F. M. *et al.* Graphene-based nanomaterials: biological and medical applications and toxicity. *Nanomedicine* **10,** 2423–2450 (2015).

3. Shen, H., Zhang, L., Liu, M. & Zhang, Z. Biomedical Applications of Graphene. *Theranostics* **2,** 283–294 (2012).

4. Novoselov, K. S. *et al.* Electric field in atomically thin carbon films. *Science* . **306,** 666–669 (2004).

5. Geim, A. K. & Novoselov, K. S. The rise of graphene. *Nat. Mater.* **6,** 183–191 (2007).

6. Allen, M. J., Tung, V. C. & Kaner, R. B. Honeycomb Carbon: A Review of Graphene. *Chem. Rev.* **110,** 132–145 (2010).

7. Juang, Z. Y. *et al.* Graphene synthesis by chemical vapor deposition and transfer by a roll-to-roll process. *Carbon N. Y.* **48,** 3169–3174 (2010).

8. Emtsev, K. V. *et al.* Towards wafer-size graphene layers by atmospheric pressure graphitization of silicon carbide. *Nat. Mater.* **8,** 203–207 (2009).

9. Eda, G., Fanchini, G. & Chhowalla, M. Large-area ultrathin films of reduced graphene oxide as a transparent and flexible electronic material. *Nat. Nanotechnol.* **3,** 270–274 (2008).

10. David, L. *et al.* Synthesis of graphene films by rapid heating and quenching at ambient pressures and their electrochemical characterization. *ACS Appl. Mater. Interfaces* **5,** 546–552 (2013).

11. Reina, A. *et al.* Large Area, Few-Layer Graphene Films on Arbitrary Substrates by Chemical Vapor Deposition. *Nano Lett.* **9,** 30–35 (2009).

12. Meyer, J. C. *et al.* The structure of suspended graphene sheets. *Nature* **446,** 60–63 (2007).

13. Wang, Y., Li, Z., Wang, J., Li, J. & Lin, Y. Graphene and graphene oxide: Biofunctionalization and applications in biotechnology. *Trends in Biotechnology* **29,** 205–212 (2011).

14. Foldvari, M. & Bagonluri, M. Carbon nanotubes as functional excipients for nanomedicines: I. pharmaceutical properties. *Nanomedicine Nanotechnology, Biol. Med.* **4,** 173–182 (2008).

15. Li, N. *et al.* Graphene meets biology. *Chinese Sci. Bull.* **59,** 1341–1354 (2014).

16. Qiu, L., Liu, J. Z., Chang, S. L. Y. Y., Wu, Y. & Li, D. Biomimetic superelastic graphene-based cellular monoliths. *Nat. Commun.* **3,** 1241 (2012).

17. Podila, R., Moore, T., Alexis, F. & Rao, A. M. Graphene coatings for enhanced hemo-compatibility of nitinol stents. *RSC Adv.* **3,** 1660–1665 (2013).

18. Brodie, B. C. On the Atomic Weight of Graphite. *Philos. Trans. R. Soc. London* **149,** 249–259 (1859).

19. Dreyer, D. R., Park, S., Bielawski, C. W. & Ruoff, R. S. The chemistry of graphene oxide. *Chem. Soc. Rev.* **39,** 228–240 (2010).

20. Compton, O. C. & Nguyen, S. T. Graphene oxide, highly reduced graphene oxide, and graphene: Versatile building blocks for carbon-based materials. *Small* **6,** 711–723 (2010).

21. Hummers, W. S. & Offeman, R. E. Preparation of Graphitic Oxide. *J. Am. Chem. Soc.* **80,** 1339–1339 (1958).

22. Staudenmaier, L. Verfahren zur Darstellung der Graphits??ure. *Berichte der Dtsch. Chem. Gesellschaft* **31,** 1481–1487 (1898).

23. Tang, L. *et al.* Bottom-up synthesis of large-scale graphene oxide nanosheets. *J. Mater. Chem.* **22,** 5676 (2012).

24. Yu, H., Zhang, B., Bulin, C., Li, R. & Xing, R. High-efficient Synthesis of Graphene Oxide Based on Improved Hummers Method. *Sci. Rep.* **6,** 36143 (2016).

25. Johnson, J. A., Benmore, C. J., Stankovich, S. & Ruoff, R. S. A neutron diffraction study of nano-crystalline graphite oxide. *Carbon N. Y.* **47,** 2239–2243 (2009).

26. Lerf, A., He, H., Forster, M. & Klinowski, J. Structure of Graphite Oxide Revisited Ⅱ . *J. Phys. Chem. B* **102,** 4477–4482 (1998).

27. Wang, L. *et al.* Fabrication and characterization of flexible silk fibroin films reinforced with graphene oxide for biomedical applications. *RSC Adv.* **4,** 40312–40320 (2014).

28. Nurunnabi, M. *et al.* Bioapplication of graphene oxide derivatives: drug/gene delivery, imaging, polymeric modification, toxicology, therapeutics and challenges. *RSC Adv.* **5,** 42141–42161 (2015).

29. Liu, Z., Robinson, J. T., Sun, X. & Dai, H. PEGylated nanographene oxide for delivery of water-insoluble cancer drugs. *J. Am. Chem. Soc.* **130,** 10876–10877 (2008).

30. Xu, Z. *et al.* Covalent functionalization of graphene oxide with biocompatible poly(ethylene glycol) for delivery of paclitaxel. *ACS Appl. Mater. Interfaces* **6,** 17268–17276 (2014).

31. Jin, R., Ji, X., Yang, Y., Wang, H. & Cao, A. Self-assembled graphene-dextran nanohybrid for killing drug-resistant cancer cells. *ACS Appl. Mater. Interfaces* **5,** 7181–7189 (2013).

32. Zhang, L., Xia, J., Zhao, Q., Liu, L. & Zhang, Z. Functional graphene oxide as a nanocarrier for controlled loading and targeted delivery of mixed anticancer drugs. *Small* **6,** 537–544 (2010).

33. Zhou, L. *et al.* Graphene oxide noncovalent photosensitizer and its anticancer activity in vitro. *Chem. - A Eur. J.* **17,** 12084–12091 (2011).

34. Rana, V. K. *et al.* Synthesis and drug-delivery behavior of chitosan-functionalized graphene oxide hybrid nanosheets. *Macromol. Mater. Eng.* **296,** 131–140 (2011).

35. Lin, J., Chen, X. & Huang, P. Graphene-based nanomaterials for bioimaging. *Adv. Drug Deliv. Rev.* **105,** 242–254 (2016).

36. Janib, S. M., Moses, A. S. & MacKay, J. A. Imaging and drug delivery using theranostic nanoparticles. *Adv. Drug Deliv. Rev.* **62,** 1052–1063 (2010).

37. Yang, K., Feng, L., Shi, X. & Liu, Z. Nano-graphene in biomedicine: theranostic applications. *Chem. Soc. Rev.* **42,** 530–47 (2013).

38. Sun, X. *et al.* Nano-Graphene Oxide for Cellular Imaging and Drug Delivery. *NANO Res.* **1,** 203–212 (2008).

39. Yang, K. *et al.* Graphene in Mice: Ultrahigh In Vivo Tumor Uptake and Efficient Photothermal Therapy. *Nano Lett.* **10,** 3318–3323 (2010).

40. Langer, R. & Vacanti, J. Tissue engineering. *Science.* **260,** 920–926 (1993).

41. Resende, R. R. *et al.* Scale/Topography of Substrates Surface Resembling Extracellular Matrix for Tissue Engineering. *J. Biomed. Nanotechnol.* **10,** 1157–1193 (2014).

42. Cha, C. *et al.* Controlling Mechanical Properties of Cell-Laden Hydrogels by Covalent Incorporation of Graphene Oxide. *Small* **10,** 514–523 (2014).

43. Shin, S. R. *et al.* Cell-laden Microengineered and Mechanically Tunable Hybrid Hydrogels of Gelatin and Graphene Oxide. *Adv. Mater.* **25,** 6385–6391 (2013).

44. da Silva, E. E. *et al.* Nanostructured 3-D collagen/nanotube biocomposites for future bone regeneration scaffolds. *Nano Res.* **2,** 462–473 (2009).

45. Geetha Bai, R., Ninan, N., Muthoosamy, K. & Manickam, S. Graphene: A versatile platform for nanotheranostics and tissue engineering. *Prog. Mater. Sci.* **91,** 24–69 (2018).

46. Xie, X. *et al.* Graphene and hydroxyapatite self-assemble into homogeneous, free standing nanocomposite hydrogels for bone tissue engineering. *Nanoscale* **7,** 7992–8002 (2015).

47. Faghihi, S., Karimi, A., Jamadi, M., Imani, R. & Salarian, R. Graphene oxide/poly(acrylic acid)/gelatin nanocomposite hydrogel: Experimental and numerical validation of hyperelastic model. *Mater. Sci. Eng. C* **38,** 299–305 (2014).

48. Depan, D., Girase, B., Shah, J. S. & Misra, R. D. K. Structure–process–property relationship of the polar graphene oxide-mediated cellular response and stimulated growth of osteoblasts on hybrid chitosan network structure nanocomposite scaffolds. *Acta Biomater.* **7,** 3432–3445 (2011).

49. Park, S. *et al.* Biocompatible, Robust Free-Standing Paper Composed of a TWEEN/Graphene Composite. *Adv. Mater.* **22,** 1736–1740 (2010).

50. Guo, W. *et al.* Self-Powered Electrical Stimulation for Enhancing Neural Differentiation of Mesenchymal Stem Cells on Graphene–Poly(3,4-ethylenedioxythiophene) Hybrid Microfibers. *ACS Nano* **10,** 5086–5095 (2016).

51. Guo, M. *et al.* N-containing functional groups induced superior cytocompatible and hemocompatible graphene by NH2ion implantation. *J. Mater. Sci. Mater. Med.* **24,** 2741–2748 (2013).

52. Ku, S. H. & Park, C. B. Myoblast differentiation on graphene oxide. *Biomaterials* **34,** 2017–2023 (2013).

53. Lee, W. C. *et al.* Origin of Enhanced Stem Cell Growth and Differentiation on Graphene and Graphene Oxide. *ACS Nano* **5,** 7334–7341 (2011).

54. Liu, H. *et al.* Gelatin functionalized graphene oxide for mineralization of hydroxyapatite: biomimetic and in vitro evaluation. *Nanoscale* **6,** 5315 (2014).

55. Liu, H. *et al.* Biomimetic and cell-mediated mineralization of hydroxyapatite by carrageenan functionalized graphene oxide. *ACS Appl. Mater. Interfaces* **6,** 3132–3140 (2014).

56. Zhao, H. *et al.* Graphene-based nanomaterials for drug and/or gene delivery, bioimaging, and tissue engineering. *Drug Discovery Today* **22,** 1302–1317 (2017).

57. Teimouri, M., Nia, A. H., Abnous, K., Eshghi, H. & Ramezani, M. Graphene oxide–cationic polymer conjugates: Synthesis and application as gene delivery vectors. *Plasmid* **84–85,** 51–60 (2016).

58. Feng, L., Zhang, S. & Liu, Z. Graphene based gene transfection. *Nanoscale* **3,** 1252 (2011).

59. Kim, H., Namgung, R., Singha, K., Oh, I.-K. & Kim, W. J. Graphene Oxide-Polyethylenimine Nanoconstruct as a Gene Delivery Vector and Bioimaging Tool. *Bioconjug. Chem.* **22,** 2558–2567 (2011).

60. Zhang, J. *et al.* Dual-Polymer-Functionalized Nanoscale Graphene Oxide as a Highly Effective Gene Transfection Agent for Insect Cells with Cell-Type-Dependent Cellular Uptake Mechanisms. *Part. Part. Syst. Charact.* **30,** 794–803 (2013).

61. Ou, L. *et al.* Toxicity of graphene-family nanoparticles: A general review of the origins and mechanisms. *Particle and Fibre Toxicology* **13,** (2016).

62. Li, Y. *et al.* The triggering of apoptosis in macrophages by pristine graphene through the MAPK and TGF-beta signaling pathways. *Biomaterials* **33,** 402–411 (2012).

63. Zhang, Y. *et al.* Cytotoxicity effects of graphene and single-wall carbon nanotubes in neural phaeochromocytoma-derived pc12 cells. *ACS Nano* **4,** 3181–3186 (2010).

64. Linares, J. *et al.* Endocytic Mechanisms of Graphene Oxide Nanosheets in Osteoblasts, Hepatocytes and Macrophages. *ACS Appl. Mater. Interfaces* **6,** 13697–13706 (2014).

65. Sydlik, S. A., Jhunjhunwala, S., Webber, M. J., Anderson, D. G. & Langer, R. In vivo compatibility of graphene oxide with differing Oxidation states. *ACS Nano* **9,** 3866–3874 (2015).

66. Gratton, S. E. A. *et al.* The effect of particle design on cellular internalization pathways. *Proc. Natl. Acad. Sci.* **105,** 11613–11618 (2008).

67. Mullick Chowdhury, S. *et al.* Cell specific cytotoxicity and uptake of graphene nanoribbons. *Biomaterials* **34,** 283–293 (2013).

68. Chatterjee, N., Eom, H. J. & Choi, J. A systems toxicology approach to the surface functionality control of graphene-cell interactions. *Biomaterials* **35,** 1109–1127 (2014).

69. Li, Y. *et al.* Graphene microsheets enter cells through spontaneous membrane penetration at edge asperities and corner sites. *Proc. Natl. Acad. Sci.* **110,** 12295–12300 (2013).

70. Horváth, L. *et al.* Evaluation of the toxicity of graphene derivatives on cells of the lung luminal surface. *Carbon N. Y.* **64,** 45–60 (2013).

71. Chang, Y. *et al.* In vitro toxicity evaluation of graphene oxide on A549 cells. *Toxicol. Lett.* **200,** 201–210 (2011).

72. Boya, P., Reggiori, F. & Codogno, P. Emerging regulation and functions of autophagy. *Nat. Cell Biol.* **15,** 713–720 (2013).

73. Mizushima, N., Yoshimori, T. & Levine, B. Methods in Mammalian Autophagy Research. *Cell* **140,** 313–326 (2010).

74. Stern, S. T. & Johnson, D. N. Role for nanomaterial-autophagy interaction in neurodegenerative disease. *Autophagy* **4,** 1097–100 (2008).

75. Chen, G.-Y. *et al.* Simultaneous induction of autophagy and toll-like receptor signaling pathways by graphene oxide. *Biomaterials* **33,** 6559–6569 (2012).

76. Bakandritsos, A. *et al.* Cyanographene and Graphene Acid: Emerging Derivatives Enabling High-Yield and Selective Functionalization of Graphene. *ACS Nano* **11,** 2982–2991 (2017).

77. Kastler, M. *et al.* Organization of Charge-Carrier Pathways for Organic Electronics. *Adv. Mater.* **18,** 2255–2259 (2006).

78. Oparka, M. *et al.* Quantifying ROS levels using CM-H2DCFDA and HyPer. *Methods* **109,** 3–11 (2016).

79. Wang, K. *et al.* Biocompatibility of Graphene Oxide. *Nanoscale Res. Lett.* (2010)

80. Lewinski, N., Colvin, V. & Drezek, R. Cytotoxicity of Nanoparticles. *Small* **4,** 26–49 (2008).

81. Feng, L., Zhang, S. & Liu, Z. Graphene based gene transfection. *Nanoscale* **3,** 1252–1257 (2011).